Eur. Phys. J. B **83**, 301–317 (2011)
DOI: 10.1140/epjb/e2011-20351-3

THE EUROPEAN PHYSICAL JOURNAL B

Colloquium

Klein tunneling in graphene: optics with massless electrons

P.E. Allain[1] and J.N. Fuchs[2,a]

[1] Institut d'Électronique Fondamentale, Univ. Paris-Sud, CNRS UMR 8622, 91405 Orsay, France
[2] Laboratoire de Physique des Solides, Univ. Paris-Sud, CNRS, UMR 8502, 91405 Orsay, France

Received 6 May 2011 / Received in final form 17 August 2011
Published online 10 October 2011 –

Abstract. This article provides a pedagogical review on Klein tunneling in graphene, i.e. the peculiar tunneling properties of two-dimensional massless Dirac electrons. We consider two simple situations in detail: a massless Dirac electron incident either on a potential step or on a potential barrier and use elementary quantum wave mechanics to obtain the transmission probability. We emphasize the connection to related phenomena in optics, such as the Snell-Descartes law of refraction, total internal reflection, Fabry-Pérot resonances, negative refraction index materials (the so called meta-materials), etc. We also stress that Klein tunneling is not a genuine quantum tunneling effect as it does not necessarily involve passing through a classically forbidden region via evanescent waves. A crucial role in Klein tunneling is played by the conservation of (sublattice) pseudo-spin, which is discussed in detail. A major consequence is the absence of backscattering at normal incidence, of which we give a new shorten proof. The current experimental status is also thoroughly reviewed. The Appendix contains the discussion of a one-dimensional toy model that clearly illustrates the difference in Klein tunneling between mono- and bi-layer graphene.

1 Introduction

The tunnel effect of a particle going through a potential barrier is now a standard exercise in elementary quantum mechanics, which goes back to the early days of this theory [1–3]. It is usually obtained by solving the Schrödinger equation either approximately with the semi-classical WKB method or exactly for piecewise constant (square) potentials [4]. The probability for the particle to cross the potential barrier decays exponentially with the width and the energy height of the barrier. Thus, even if classically the probability to go through the barrier is equal to zero, quantum dynamics allows the crossing with a tiny probability. The mechanism behind quantum tunneling is the possibility for a quantum particle to enter a classically forbidden regions as permitted by Heisenberg's uncertainty principle. This is possible thanks to evanescent waves.

However it would be considered paradoxical for a particle to tunnel with certainty regardless of the height and the width of the barrier. It turns out that such an effect has been described theoretically by the Swedish physicist Oskar Klein in 1929 [5,6] for relativistic electrons using the three dimensional (3D) massive Dirac equation (i.e. the original Dirac equation describing a relativistic massive electron [7,8] in ordinary space). This effect has since been know as the "Klein paradox".

Recently a similar effect, though for 2D massless Dirac electrons, has been predicted [9] (see also [10] and [11]) and evidences of its observation in a graphene sheet were reported [12–15]. The latter is now known as the "Klein tunnel effect" or "Klein tunneling".

The aim of the present article is to review this effect and to present simple derivations that can easily be reproduced in order to demystify it. In particular, we wish to emphasize that the "Klein tunnel effect" is *not* a tunnel effect in the usual quantum mechanical sense as it does not crucially rely on evanescent waves and that it is not paradoxical (at least from the solid state physics perspective). For example, there is no problem with charge conservation as often stated in the context of the Klein paradox. We also give simple physical arguments in order to understand the unusual tunneling behavior of massless Dirac particles and stress the crucial importance of the (sublattice) pseudo-spin conservation.

The article is organized as follows. In Section 2, we review the low-energy effective theory of valence electrons in graphene and then discuss properties of the 2D massless Dirac equations that are to be used in the following sections. In particular, we emphasize the importance of the pseudo-spin conservation and prove that it implies the absence of backscattering at normal incidence on any potential profile. Section 3 discusses the case of a massless Dirac electron incident on a potential step (both sharp and smooth) and Section 4 that of a square potential barrier. In Section 5, we review in detail the current status of experiments on Klein tunneling. Conclusions are given in Section 6. An Appendix treats Klein tunneling in 1D using a toy model that allows us to easily compare mono- and bi-layer graphene.

[a] e-mail: fuchs@lps.u-psud.fr

We mention the following reviews on the Klein paradox by Calogeracos and Dombey [6,16] and more recently on Klein tunneling in graphene by Beenakker [17] and by Pereira et al. [18].

2 Two-dimensional massless Dirac equation in graphene

2.1 Low energy description of electrons in graphene

We start by briefly reviewing the low-energy effective description of valence electrons in a graphene flake. Graphene is a two dimensional honeycomb crystal of carbon atoms. The honeycomb crystal is however not a Bravais lattice. It is made out of a triangular Bravais lattice with a two atom basis (usually called A and B). This can alternately be seen as two triangular sublattices. As a consequence of this two-site basis, the electronic wavefunction is a bispinor: in other words, the electron carries – in addition to its usual spin 1/2, which we shall neglect in the following – a pseudo-spin 1/2 associated with its sublattice degree of freedom. We shall refer to it as sublattice pseudo-spin. The electronic band structure of graphene is usually obtained in the nearest-neighbor tight-binding model [19]. Conduction (or π) electrons are allowed to jump from the $2p_z$ orbital of a carbon atom to one of its three nearest neighbors with hopping amplitude (a.k.a. as resonance integral) $\gamma \equiv t \approx 3$ eV. The following dispersion relation results (see Fig. 1):

$$E = \pm\gamma\sqrt{\left(1 + 4\cos^2\left(k_y a\right) + 4\cos\left(k_y a\right)\cos\left(k_x\sqrt{3}a\right)\right)} \tag{1}$$

where the lattice constant $a \approx 2.46$ Å and the carbon-carbon distance is $a/\sqrt{3} \approx 1.42$ Å. Conduction (CB, $\alpha = +1$) and valence bands (VB, $\alpha = -1$), respectively, correspond to the different signs in the above dispersion relation ($\alpha = \pm 1$ is called the band index); they touch at two inequivalent points – Dirac points or valleys K and K' – which are at the corners of the hexagonal Brillouin zone in reciprocal space (see Fig. 1). These K and K' points are separated by a distance $\sim 1/a$ in reciprocal space.

In the vicinity of the Dirac points the energy depends linearly on the wave number, similarly to a massless relativistic (or ultra-relativistic) particle (see Fig. 1). As a consequence, at low energies, and close to the K and K' points, the electrons can be described by a 2D massless Dirac eigenvalue equation:

$$-i\hbar v_F \hat{\boldsymbol{\sigma}} \cdot \boldsymbol{\nabla}\psi(\mathbf{r}) = E\psi(\mathbf{r}). \tag{2}$$

A detailed derivation of this linearized equation starting from the tight-binding model can be found, for example, in [20]. Here $v_F \equiv \sqrt{3}\gamma a/(2\hbar) \approx 10^6$ m/s is the Fermi velocity in graphene which plays the role of an effective velocity of light; $\hat{\boldsymbol{\sigma}} \equiv (\hat{\sigma}_x, \hat{\sigma}_y)$ is the 2D vector of Pauli matrices, $\psi(\mathbf{r}) = (\psi_A(\mathbf{r}), \psi_B(\mathbf{r}))$ is the two-component (bi-spinor) wavefunction of the electron, E its energy and $\boldsymbol{p} \to -i\hbar\boldsymbol{\nabla}$ is the momentum operator in the position representation[1]. The two components of the wavefunction refer to the two atoms A and B in the unit cell. There are actually two such Dirac equations: one for each Dirac point or valley (K or K'). In the following, we only consider a single Dirac cone, as if we could separate the K and K' valleys. This is a valid approximation if intervalley scattering is unlikely, which is the case if the potential changes are smooth on the lattice scale. This point is discussed in more detail below, see Section 2.3. The effective description in terms of massless Dirac electrons is valid only for energies smaller than the bandwidth $\gamma \sim 3$ eV.

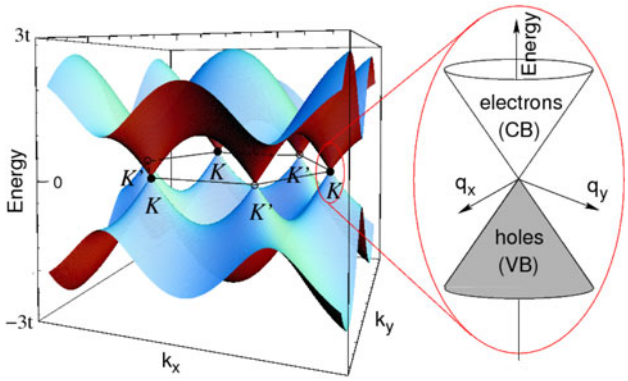

Fig. 1. Band structure of graphene as computed in the tight-binding model of Wallace [19]. The energy E is shown as a function of the two dimensional Bloch wavevector (k_x, k_y). In the vicinity of the Dirac points at the two inequivalent corners K and K' of the hexagonal Brillouin zone, the dispersion relation is linear and hence locally equivalent to a Dirac cone (see the zoomed region). In undoped graphene, the Fermi energy lies exactly at the two Dirac points and the Fermi surface consists of just two points: the valence band (VB) is filled with electrons and the conduction band (CB) is empty. From a band theory perspective, undoped graphene is therefore a zero gap semiconductor. However, as it is experimentally found that it still conducts electricity at the lowest attainable temperatures (with a conductivity of the order of a few times the conductance quantum e^2/h), it is better called a (zero band overlap) semi-metal. [Figure courtesy of Mark Goerbig].

For a general reference on graphene see [21] and for a pedagogical introduction see [22,23].

2.2 Eigenstates of the 2D massless Dirac Hamiltonian

In matrix notation, the two-dimensional massless Dirac Hamiltonian is given by:

$$\hat{H}_{\text{kin}} = \hbar v_F \boldsymbol{k}.\hat{\boldsymbol{\sigma}} = \hbar v_F \begin{pmatrix} 0 & k_x - ik_y \\ k_x + ik_y & 0 \end{pmatrix} \tag{3}$$

where hats $\hat{}$ denote 2×2 matrices in sublattice space (A, B) and the index "kin" refers to the kinetic energy.

[1] Note that in the low energy effective description, the wavevector $\boldsymbol{k}$ and the corresponding momentum $\boldsymbol{p} = \hbar\boldsymbol{k}$ are now defined from the K or K' point and no more from the center Γ of the Brillouin zone. The restriction to low energy also means that $|\boldsymbol{k}| \ll 1/a$.

For simplicity, in the following, we use units such that $\hbar \equiv 1$ and $v_F \equiv 1$, therefore energies and wavevectors are equal. As it will be useful when considering piecewise constant potentials, we add a constant potential to this Hamiltonian (which simply amounts to shifting the zero of energy):

$$\hat{H} = \hat{H}_{\text{kin}} + V_0\hat{1} = \begin{pmatrix} V_0 & k_x - ik_y \\ k_x + ik_y & V_0 \end{pmatrix} \tag{4}$$

$\hat{H}$ corresponds to the total energy, $\hat{H}_{\text{kin}}$ to the kinetic energy and $V_0\hat{1}$ to the potential energy, where $\hat{1}$ is the unit 2×2 matrix. From equation (4) we have the eigenvalue equation: $\hat{H}_{\text{kin}}|\psi\rangle = E_{\text{kin}}|\psi\rangle$ where $E_{\text{kin}} = E - V_0$. An eigenstate $|\psi\rangle$ corresponds to a plane wave, which we write:

$$\psi(\boldsymbol{r}) = e^{i\boldsymbol{k}.\boldsymbol{r}}\begin{pmatrix} u \\ v \end{pmatrix} = \langle \boldsymbol{r}|\psi\rangle \tag{5}$$

where $\boldsymbol{k} = (k_x, k_y)$ is the wavevector and the bispinor is given by u (respectively v), which is the complex amplitude on the A (resp. B) sublattice. The corresponding kinetic energy is such that $E_{\text{kin}}^2 = k_x^2 + k_y^2$. In the following, we assume k_y to be real and positive (i.e. a plane wave propagative from left $y < 0$ to right $y > 0$). However, k_x can be real or purely imaginary, because k_x^2 can be positive or negative. If k_x is real, the wave is oscillating. If k_x is purely imaginary, the wave is evanescent.

2.2.1 Oscillating wave

If ${k_x}^2 > 0$ (i.e. $E_{\text{kin}}^2 > k_y^2$), the wave is oscillating and the wavefunction reads:

$$\psi = e^{i\boldsymbol{k}.\boldsymbol{r}}\frac{1}{\sqrt{2\mathcal{A}}}\begin{pmatrix} 1 \\ \alpha e^{i\phi} \end{pmatrix} = \langle \boldsymbol{r}|\boldsymbol{k}, \alpha\rangle \tag{6}$$

where $\alpha = \text{sgn}(E_{\text{kin}})$ is the band index ($\alpha = 1$ in the conduction band and -1 in the valence band) and ϕ is the angle between the wave vector $\boldsymbol{k}$ and the x-axis such that $\tan\phi = k_y/k_x$. The kinetic energy is $E_{\text{kin}} = E - V_0 = \alpha\sqrt{{k_y}^2 + {k_x}^2}$,with ${k_y}^2 + {k_x}^2 > 0$. The total surface $\mathcal{A}$ of the graphene sheet is taken to be one in the following $\mathcal{A} \equiv 1$.

2.2.2 Evanescent wave

An interesting possibility is that k_x^2 be negative (i.e. $E_{\text{kin}}^2 < k_y^2$), then $k_x = \pm i\kappa$, with $\kappa \in \mathbb{R}^+$. We need to consider two possibilities depending on E_{kin}.

– If $E_{\text{kin}} \neq 0$, there are two sub-cases depending on the sign of $|k_x|$. On the one hand, if $k_x = i\kappa$

$$\psi \sim e^{ik_y y}e^{-\kappa x}\begin{pmatrix} 1 \\ \alpha i\sqrt{\frac{k_y+\kappa}{k_y-\kappa}} \end{pmatrix} \tag{7}$$

and $E_{\text{kin}} = E - V_0 = \alpha\sqrt{k_y^2 - \kappa^2}$, with $k_y^2 - \kappa^2 > 0$ and $\alpha = \text{sgn}(E - V_0)$. This wave decays towards increasing x. On the other hand, if $k_x = -i\kappa$

$$\psi \sim e^{ik_y y}e^{\kappa x}\begin{pmatrix} 1 \\ \alpha i\sqrt{\frac{k_y-\kappa}{k_y+\kappa}} \end{pmatrix} \tag{8}$$

and $E_{\text{kin}} = E - V_0 = \alpha\sqrt{{k_y}^2 - \kappa^2}$, with ${k_y}^2 - \kappa^2 > 0$ and $\alpha = \text{sgn}(E - V_0)$. This wave decays towards decreasing x.

– If $E_{\text{kin}} = 0$ (i.e. $k_x^2 + k_y^2 = 0$), again two sub-cases occur. On the one hand, if $k_x = ik_y$:

$$\psi \sim e^{ik_y y}e^{-k_y x}\begin{pmatrix} 0 \\ 1 \end{pmatrix}. \tag{9}$$

On the other hand, if $k_x = -ik_y$:

$$\psi \sim e^{ik_y y}e^{k_y x}\begin{pmatrix} 1 \\ 0 \end{pmatrix}. \tag{10}$$

These solutions will be useful in the following when considering piecewise constant potentials.

2.3 Potential steps and barriers in graphene

We consider a potential step $V(\boldsymbol{r})$ and call w the characteristic length scale over which it varies. In graphene, it is possible to realize potential steps that are smooth ($w \gg a$) on the lattice scale $a \sim 0.2$ nm and therefore do not induce inter-valley scattering as the distance between valleys in reciprocal space is $|\boldsymbol{K} - \boldsymbol{K}'| \sim 1/a$ and the Fourier transform of the potential $\tilde{V}(\boldsymbol{q})$ is non-zero only for $q \ll 1/a$. For such potentials, valleys are decoupled and electrons in graphene can be described by a single valley 2D massless Dirac Hamiltonian $\hat{H} = \hat{H}_{\text{kin}} + \hat{V}(x, y)$ [24]. In addition, as the potential varies slowly over the distance between two neighboring atoms (A and B), the potential matrix $\hat{V}(x, y)$ can be taken to be diagonal in the sublattice space $V(x, y)\hat{1}$ [24]. In the following, we will consider potentials that are translationally invariant along y and therefore of the form $V(x)\hat{1}$. Therefore the complete Hamiltonian reads:

$$\hat{H} = \hat{H}_{\text{kin}} + V(x)\hat{1} = \boldsymbol{k} \cdot \hat{\boldsymbol{\sigma}} + V(x)\hat{1}. \tag{11}$$

In addition, the potential can be smooth ($w \gg 1/k_F$) or sharp ($w \ll 1/k_F$) on the Fermi wavelength scale $1/k_F = 1/|E_{\text{kin}}|$. If it is sharp, we can assume that it is piecewise constant ("square"). For example, $V(x) = V_0\Theta(x)$ for a square step (see Fig. 2) and $V(x) = V_0\Theta(x)\Theta(d - x)$ for a square barrier (see Fig. 8), where Θ is the Heaviside step function. The case of a sharp step is discussed in Section 3.1, that of a smooth step (see Fig. 6) in Section 3.3 and that of a sharp barrier in Section 4.

Depending on the doping (the position of the Fermi level), the steps and barriers can correspond to different

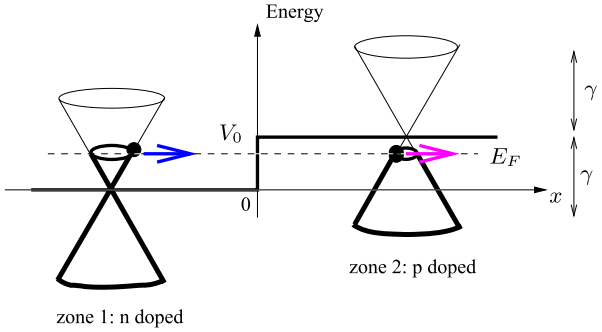

Fig. 2. Band structure across a square potential step V_0 (or sharp np junction). At equilibrium the chemical potential is uniform $\mu(T=0) = E_F$: the Fermi level is shown as a dashed line. The black dot represents the electron before and after the step: its direction of motion is indicated by a blue arrow. Note that its wavevector is reversed but not its velocity. The typical bandwidth $\gamma \sim 3$ eV is also shown.

types of junctions. If the doping is such that the Fermi level lies in different bands before and after the step, the junction is said to be bipolar (np or pn junction). If it lies in the same band, the junction is said to be unipolar (nn' or pp' junction). Similarly barriers can correspond to bipolar (npn or pnp) or unipolar ($nn'n$ or $pp'p$) junctions. In the following we will consider np or nn' junctions (steps) and npn or $nn'n$ junctions (barriers).

2.4 Velocity and probability current

For later purpose, we define the average velocity and the average probability current of an eigenstate $|\boldsymbol{k}, \alpha\rangle$. Using the Heisenberg equation of motion, the velocity operator can be evaluated as:

$$\hat{\boldsymbol{v}} \equiv \dot{\boldsymbol{r}} = \frac{1}{i}[\boldsymbol{r}, \hat{H}] = \hat{\boldsymbol{\sigma}}. \tag{12}$$

From which, one can obtain the average velocity of a plane wave of momentum $\boldsymbol{k}$ and band index α:

$$\boldsymbol{v} \equiv \langle \boldsymbol{k}, \alpha | \hat{\boldsymbol{v}} | \boldsymbol{k}, \alpha \rangle = \alpha \frac{\boldsymbol{k}}{k}. \tag{13}$$

Hence in the case where the band index is $\alpha = -1$ – i.e. when the electron is in the valence band and has a negative kinetic energy $E_{\text{kin}} = E - V_0 < 0$ – the wavector is opposite to the propagation of the wave (i.e. to the velocity), which is quite unusual.

The average current is obtained in the following way. The probability density of the state $|\psi\rangle$ is $|\psi(\boldsymbol{r}, t)|^2$ and the associated (average) probability current is called $\boldsymbol{j}(\boldsymbol{r}, t)$. The conservation of probability

$$\boldsymbol{\nabla} \cdot \boldsymbol{j} = -\frac{\partial}{\partial t}|\psi|^2 \tag{14}$$

allows us to define the average current as:

$$\boldsymbol{j} = \psi^\dagger \hat{\boldsymbol{\sigma}} \psi. \tag{15}$$

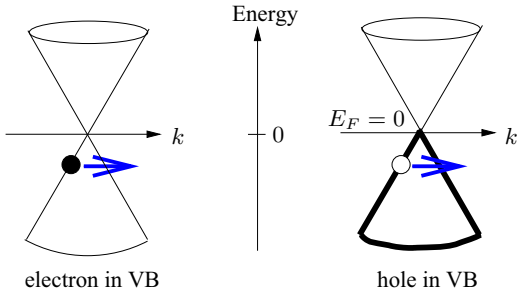

Fig. 3. Difference between an electron and a hole both in the valence band (VB). We compare an electron of momentum $\boldsymbol{k}_e$ in the VB (on the left) with a hole that corresponds to removing an electron of momentum $\boldsymbol{k}_e$ in an otherwise filled VB (on the right). The electron has a negative kinetic energy $E_e = -k_e$, a negative charge $-e$, an average velocity $\langle \boldsymbol{v}_e \rangle = -\boldsymbol{k}_e/k_e$ opposite to its momentum and carries an electric current $-e\langle \boldsymbol{v}_e \rangle$. The hole has a momentum opposite to that of the electron $\boldsymbol{k}_t = -\boldsymbol{k}_e$, its kinetic energy is positive $E_t = k_t = -E_e$, its charge is positive $+e$, its average velocity is the same as that of the electron $\langle \boldsymbol{v}_t \rangle = \boldsymbol{k}_t/k_t = \langle \boldsymbol{v}_e \rangle$ (therefore it moves in the same direction as the electron) and its electric current is opposite $+e\langle \boldsymbol{v}_t \rangle$. The blue arrow indicates the direction of motion.

The average velocity is given by:

$$\langle \psi | \hat{\boldsymbol{v}} | \psi \rangle = \int d^2 r \, \psi^\dagger \hat{\boldsymbol{\sigma}} \psi = \int d^2 r \, \boldsymbol{j}. \tag{16}$$

For an eigenstate $|\boldsymbol{k}, \alpha\rangle$, the average current reads:

$$\boldsymbol{j} = \alpha \frac{\boldsymbol{k}}{k} \tag{17}$$

which is just equal to the average velocity as we took a unit system area $\mathcal{A} \equiv 1$.

2.5 Electron versus hole in the valence band

An electron moving in the valence band (VB) should not be confused with a hole, which is the absence of an electron in an otherwise filled band (see Fig. 3). Let us compare an electron of momentum $\boldsymbol{k}_e$ in an otherwise empty VB with a hole that corresponds to removing of an electron of momentum $\boldsymbol{k}_e$ in an otherwise filled VB. The electron has a negative kinetic energy $E_e = -k_e$ (as measured from the Dirac point), a negative charge $-e$, an average velocity $\langle \boldsymbol{v}_e \rangle = -\boldsymbol{k}_e/k_e$ opposite to its momentum and carries an electric current $-e\langle \boldsymbol{v}_e \rangle$. Concerning the hole, its momentum is opposite to that of the electron $\boldsymbol{k}_t = -\boldsymbol{k}_e$ [2], its kinetic energy is positive $E_t = k_t = -E_e$, its charge is positive $+e$, its average velocity is the same as that of the

[2] Despite the fact that in Figure 3 the hole appears to be at the same position (in reciprocal space) as the electron, its momentum is opposite $\boldsymbol{k}_t = -\boldsymbol{k}_e$. This is due to the fact that the hole corresponds to the *removal* of an electron. The same remark applies to the kinetic energy $E_t = -E_e$ as measured from the Dirac point (band crossing).

electron $\langle \boldsymbol{v}_t \rangle = \boldsymbol{k}_t/k_t = \langle \boldsymbol{v}_e \rangle$ (therefore it moves in the same direction as the electron) and its electric current is opposite $+e\langle \boldsymbol{v}_t \rangle$.

Let us now discuss Klein tunneling for an electron (initially in the conduction band (CB)) incident on a step (see Fig. 2). The electron is transmitted inside the step as an electron in the VB and not as a hole (as often stated). Conservation of the electric current should be enough to understand that point. Note that in order to keep moving in the same direction, the electron has to reverse its momentum when going from the CB (outside the step) to the VB (inside the step).

2.6 General conservation laws: energy E, momentum projection k_y and 1D current j_x

There are three fundamental conservation laws that we will keep on using when considering a massless Dirac particle incident on a potential step or barrier that is translationally invariant in the y direction $\hat{V}(x,y) = V(x)\hat{1}$. First, there is the conservation of energy E as a result of time translational invariance. Then, the momentum projection k_y is also conserved as a result of translational invariance along y (i.e. parallel to the interface(s)). Finally, since the system is time independent, the probability conservation law reads $\boldsymbol{\nabla} \cdot \boldsymbol{j} = 0$ and translational invariance along y further implies that $\boldsymbol{j}(x,y) = \boldsymbol{j}(x)$ and therefore that the 1D current is conserved:

$$j_x(x) = \text{const.} \tag{18}$$

2.7 Conservation of pseudo-spin and the absence of backscattering

2.7.1 Pseudo-spin and chirality (or helicity)

An electron described by the 2D massless Dirac equation carries a pseudo-spin 1/2 related to its freedom of belonging either to the A or to the B sublattice. In graphene, the electron has still an extra spin-type degree of freedom. It is related to its freedom of being either close to the K point or to the K' point in the Brillouin zone: this is called valley pseudo-spin. In the present paper, we do not discuss this degree of freedom and rather concentrate on the sublattice pseudo-spin $\boldsymbol{\sigma}$. The fact that the electron has a sublattice pseudo-spin is encoded in its wavefunction being a bispinor and the Hamiltonian $\hat{H}_{\text{kin}} = \boldsymbol{k} \cdot \hat{\boldsymbol{\sigma}}$ being a 2×2 matrix in sublattice space. Chirality is here defined as follows. The chirality (or helicity) operator is the projection of the sublattice pseudo-spin operator on the momentum direction:

$$\hat{C} \equiv \frac{\boldsymbol{k} \cdot \hat{\boldsymbol{\sigma}}}{k}. \tag{19}$$

Its eigenvalues are $C = \pm 1$. When there is no potential $\hat{V}(\boldsymbol{r}) = 0$, the chirality operator commutes with the Hamiltonian and is therefore a conserved quantity. The Hamiltonian and the chirality can be diagonalized by the same eigenvectors:

$$\hat{C}|\boldsymbol{k}, \alpha\rangle = \alpha|\boldsymbol{k}, \alpha\rangle \tag{20}$$

which shows that the chirality C is just the band index α in that case[3].

2.7.2 Chirality factor and the absence of backscattering

Here, we discuss an important consequence of the pseudo-spin, first discovered by Ando and coworkers in the context of carbon nanotubes [25,26]. Consider a massless Dirac electron, which is incident on an impurity whose potential is smooth on the lattice scale such that intervalley scattering is suppressed and the problem can be described within a single valley model (see Sect. 2.3). The impurity potential is therefore $\hat{V}_{\text{imp}}(\boldsymbol{r}) \approx U(\boldsymbol{r})\hat{1}$ [25,26]. For simplicity, though the argument can be made much more general (see [25,26] and the next paragraph), we will compute the scattering probability using the first order Born approximation. It is given by

$$P(\theta) \propto |\langle \boldsymbol{k'}, \alpha'|U(\boldsymbol{r})\hat{1}|\boldsymbol{k}, \alpha\rangle|^2 \tag{21}$$

where $|\boldsymbol{k}, \alpha\rangle$ and $|\boldsymbol{k'}, \alpha'\rangle$ are the initial and the final states respectively and θ is the angle between the final and initial wavevectors. As the collision is elastic $k' = k$ and $\alpha' = \alpha$. Therefore the only freedom in the final state is the angle $\theta \equiv \phi_{\boldsymbol{k'}} - \phi_{\boldsymbol{k}}$ that $\boldsymbol{k'}$ makes with $\boldsymbol{k}$. We are now in a position to compute the matrix element:

$$\langle \boldsymbol{k'}, \alpha'|U(\boldsymbol{r})\hat{1}|\boldsymbol{k}, \alpha\rangle = \frac{1 + e^{i\theta}}{2}\tilde{U}(\boldsymbol{k'} - \boldsymbol{k}) \tag{22}$$

where $\tilde{U}(\boldsymbol{q}) \equiv \int d^2r U(\boldsymbol{r}) \exp(i\boldsymbol{q} \cdot \boldsymbol{r})$ is the Fourier transform of the potential $U(\boldsymbol{r})$. Note that the transferred momentum is $q = 2k\sin(\theta/2)$. Therefore, the scattering probability reads:

$$P(\theta) \propto |\tilde{U}(\boldsymbol{q})|^2 \cos^2\frac{\theta}{2} = |\tilde{U}(\boldsymbol{q})|^2 \frac{1 + \cos\theta}{2}. \tag{23}$$

The first term $|\tilde{U}(\boldsymbol{q})|^2$ is the usual result of the Born approximation and the second $\cos^2\frac{\theta}{2}$ is due to the sublattice pseudo-spin and is called the "chirality factor". The latter is just the square of the scalar product between the incoming and outgoing bispinors: $(1, e^{i\phi_{\boldsymbol{k}}})/\sqrt{2}$ and $(1, e^{i\phi_{\boldsymbol{k'}}})/\sqrt{2}$. The effect of the chirality factor is quite dramatic as it kills backscattering ($\boldsymbol{k'} = -\boldsymbol{k}$):

$$P(\theta = \pi) \propto |\tilde{U}(\boldsymbol{q})|^2 \cos^2\frac{\pi}{2} = 0 \text{ with } q = 2k. \tag{24}$$

An intuitive explanation of this absence of backscattering is the following: if the electron tries to backscatter

[3] In the case where both valleys K and K' are considered, one finds that for an eigenstate $|\boldsymbol{k}, \alpha, \xi\rangle$ of the Hamiltonian the chirality $C = \alpha\,\xi$ is the product of the band index α and the valley index $\xi = +1$ (if K) and -1 (if K').

$\boldsymbol{k'} = -\boldsymbol{k}$ it also has to reverse its sublattice pseudo-spin $\boldsymbol{\sigma} \rightarrow -\boldsymbol{\sigma}$ as the pseudo-spin direction is tied to that of the momentum (indeed remember that away from the impurity $\hat{H}_{\text{kin}} = \boldsymbol{k} \cdot \hat{\boldsymbol{\sigma}}$). However, the potential $U(\boldsymbol{r})\hat{1}$ does not act in sublattice space (it is the unit matrix) and can therefore not reverse the pseudo-spin. Therefore backscattering is impossible. This has profound physical consequences on the transport properties of massless Dirac electrons, such as weak antilocalization [27–29].

2.7.3 Conservation of pseudo-spin and the absence of backscattering

We now prove that a 2D massless Dirac electron normally incident on a potential $V(x)\hat{1}$ can not be backscattered as a consequence of the conservation of its pseudo-spin $\hat{\sigma}_x$. We assume that the electron is initially ($t = 0$) in a momentum eigenstate ($k_x > 0, k_y = 0$) and incident on a potential that is translationally invariant in the y direction ($V(x, y) = V(x)$). It is described by the following Hamiltonian:

$$\hat{H} = k_x\hat{\sigma}_x + k_y\hat{\sigma}_y + V(x)\hat{1}. \tag{25}$$

The velocity operator in the x direction is $\hat{v}_x = -i[x, \hat{H}] = \hat{\sigma}_x$. Its time evolution is given by the Heisenberg equation of motion[4]:

$$\dot{\hat{v}}_x = -i[\hat{\sigma}_x, \hat{H}] = 2\hat{\sigma}_z k_y. \tag{26}$$

Here, because of the translational invariance along the y direction, the momentum k_y is a conserved quantity: $\dot{k}_y = -i[k_y, \hat{H}] = 0$. Therefore the momentum operator along y does not evolve $k_y(t) = k_y(0)$. If the initial state of the electron $|\psi(0)\rangle$ is an eigenstate of zero momentum in the y direction $k_y(0)|\psi(0)\rangle = 0$, then at any time $t > 0$:

$$\begin{aligned}\langle\psi(t)|\dot{\hat{v}}_x(0)|\psi(t)\rangle &= \langle\psi(0)|\dot{\hat{v}}_x(t)|\psi(0)\rangle \\ &= 2\langle\psi(0)|\hat{\sigma}_z(t)k_y(0)|\psi(0)\rangle = 0\end{aligned} \tag{27}$$

which means that the velocity (or the pseudo-spin) along x is a constant of the motion:

$$\langle\psi(t)|\hat{v}_x|\psi(t)\rangle = \langle\psi(0)|\hat{v}_x|\psi(0)\rangle = +1.$$

The electron is therefore perfectly transmitted and its motion is exactly the same as in the absence of the potential (it is not even delayed). This shows that a (single valley) massless Dirac electron normally incident on a translationally invariant potential can not be backscattered.

An alternative explanation for the absence of backscattering (invoking supersymmetry) is presented in [30].

[4] That the velocity operator does not commute with the Hamiltonian is peculiar to the Dirac equation and is responsible for the so-called zitterbewegung.

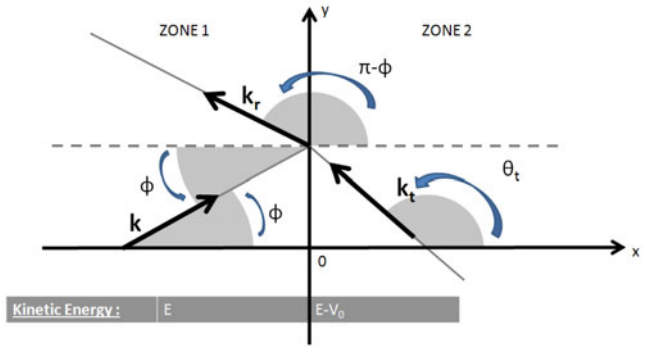

Fig. 4. An electron of energy E is incident from the left on a square potential step of height V_0 such that $V_0 > E$. Angles (ϕ and θ_t) and wavevectors in the two zones (before and after the step) are defined as follows: incident $\boldsymbol{k} = (k_x, k_y) = E(\cos\phi, \sin\phi)$; reflected $\boldsymbol{k_r} = (-k_x, k_y) = E(\cos(\pi-\phi), \sin(\pi-\phi))$; and transmitted $\boldsymbol{k_t} = (k'_x, k_y) = -(E - V_0)(\cos\theta_t, \sin\theta_t)$. ϕ is called the incidence angle.

3 Potential step

Let us first consider a square (sharp) potential step of height V_0 on which an electron of energy $E = k_F > 0$ is incident (see Fig. 2). Two zones can be defined, one for $x < 0$ corresponding to a kinetic energy of $E_{\text{kin}} = E$, another for $x > 0$ corresponding to a kinetic energy of $E_{\text{kin}} = E - V_0$. An analogy with an optical system will be made: the system is equivalent to a light beam going through a discontinuity between two transparent media. For instance, going from glass to air. Since $E > 0$ in zone 1, $\alpha = +1$; whereas, in zone 2, $\alpha = \text{sgn}(E - V_0) = \pm 1$. We consider an incoming electron with a given wavevector $\boldsymbol{k}$ in zone 1 and call $\boldsymbol{k'}$ the wavevector in zone 2. Wavevectors and angles are defined in Figure 4. In the case where the band index is -1 (i.e. when $E - V_0 < 0$) we saw that the momentum is opposite to the propagation of the wave (i.e. to the velocity), because the electron moves in the valence band. Therefore $k'_x < 0$, see Figure 4. This gives rise to anomalous refraction.

3.1 Energy below a sharp step ($0 < E < V_0$)

This corresponds to a *np* junction. From the conservation of the total energy and of the momentum projection k_y, relations between angles can be deduced. The different wavectors are written as $\boldsymbol{k}^{(j)} = (k_x^{(j)}, k_y^{(j)}) = |\boldsymbol{k}^{(j)}|(\cos\theta_j, \sin\theta_j)$, where $E_{\text{kin},j} = \alpha_j|\boldsymbol{k}^{(j)}|$ with $j = \{\text{incident, reflected, transmitted}\}$. Then the conserved wavevector projection along y reads $k_y^{(j)} = \alpha_j E_{\text{kin},j}\sin\theta_j$ and we obtain the table below:

j	incident	reflected	transmitted
Band index α_j	1	1	-1
Kinetic energy $E_{\text{kin},j}$	$E > 0$	$E > 0$	$E - V_0 < 0$
Angle θ_j	$\theta_i \equiv \phi$	θ_r	θ_t

The equality $k_y^{(i)} = k_y^{(r)}$ gives

$$\theta_r = \pi - \phi \tag{28}$$

and $k_y^{(i)} = k_y^{(t)}$ gives

$$E \sin\phi = -(E - V_0) \sin\theta_t. \tag{29}$$

This last equation can be seen as an analog of the Snell-Descartes equation for light refraction into a medium of negative refraction index n [31]. To see that the refraction index is indeed negative, one needs to define angles from the perpendicular to the interface – as is usual in optics. For the transmitted wave ("refracted ray") in zone 2, we define $\theta_2 \equiv \theta_t - \pi$ and $\theta_1 \equiv \phi$ for the incident wave in zone 1. In that case both angles θ_1 and θ_2 have a modulus smaller than $\pi/2$. Hence the Snell-Descartes law now reads $n_1 \sin\theta_1 = n_2 \sin\theta_2$ with $n_1 \propto E$ and $n_2 \propto (E - V_0) = E_{\rm kin}$ where $n_2 < 0$. Therefore the refraction index $n \propto E_{\rm kin} = \alpha k$ is proportional to the kinetic energy and may be defined as $n \equiv \alpha k a \sim E_{\rm kin}/\gamma$, where $\gamma \approx 3$ eV is the hopping amplitude (or bandwidth) and a is the lattice spacing. Note that the wavevector $k \equiv |\boldsymbol{k}|$ changes from zone 1 to zone 2, because the velocity $v_F \approx 10^6$ m/s is a constant and the kinetic energy changes from positive to negative. Another way to see that the refraction index is negative is to realize that the refraction is anomalous, or in other words that the refracted ray is closer in direction to the reflected ray than to the incident one (see Fig. 4), which is quite unusual.

In optics, the refraction index $n = c/v \propto 1/v$ is inversely proportional to the phase velocity v – where $c \approx 3 \times 10^8$ m/s is the light velocity in vacuum – which changes when going from one medium to another. As the photon (kinetic) energy is unchanged upon crossing the interface, the optical index also reads $n = k/k_0 \propto k$ where k_0 is the wavector in vacuum and k that in the medium. In optics, media with negative index of refraction – so called meta-materials – have received a lot of attention recently, see for example [32].

The next step is to write the wavefunctions in both zones 1 and 2 and to connect them on the interface at $x = 0$. Here normalization of the wavefunctions is not needed. Using equations derived in Section 2, the wave functions can be written in both zones as (see Fig. 4):

$$\psi_1 = e^{ik_y y}\left[e^{ik_x x}\begin{pmatrix}1\\ +e^{i\phi}\end{pmatrix} + re^{-ik_x x}\begin{pmatrix}1\\ +e^{i(\pi-\phi)}\end{pmatrix}\right] \tag{30}$$

$$\psi_2 = te^{ik_y y}e^{ik'_x x}\begin{pmatrix}1\\ -e^{i\theta_t}\end{pmatrix}. \tag{31}$$

The continuity of the wavefunction[5] is used in $x = 0$ to obtain:

$$1 = -r + t \text{ and } e^{i\phi} = re^{-i\phi} - te^{i\theta_t} \tag{32}$$

which gives:

$$r = \frac{e^{i\theta_t} + e^{i\phi}}{e^{-i\phi} - e^{i\theta_t}} \text{ and } t = \frac{e^{i\phi} + e^{-i\phi}}{e^{-i\phi} - e^{i\theta_t}}. \tag{33}$$

[5] For the Schrödinger equation, we would have had to use the continuity of the wavefunction and that of its derivative as well. Here the two-component spinor allows the same number of equations just from the continuity of the wavefunction.

We now wish to obtain the transmission probability T from the amplitudes r and t. This requires using the conservation of the 1D current, see equation (18), which here reads:

$$j_x[\text{incident}] + j_x[\text{reflected}] = j_x[\text{transmitted}]$$
$$\leftrightarrow \cos\phi - |r|^2 \cos\phi = -|t|^2 \cos\theta_t \tag{34}$$

and therefore:

$$1 = |r|^2 - |t|^2 \frac{\cos\theta_t}{\cos\phi}. \tag{35}$$

This is the probability conservation law $1 = R + T$. It allows one to identify the transmission T and reflection R probabilities[6] as:

$$T = -\frac{\cos\theta_t}{\cos\phi}|t|^2 \text{ and } R = |r|^2 \tag{36}$$

and we finally obtain:

$$T = -\frac{\cos\phi\cos\theta_t}{\sin^2\left(\frac{\phi+\theta_t}{2}\right)} \text{ and } R = \frac{\cos^2\left(\frac{\phi-\theta_t}{2}\right)}{\sin^2\left(\frac{\phi+\theta_t}{2}\right)} \tag{37}$$

where the transmitted angle is:

$$\theta_t = \theta_2 + \pi = \arcsin\left(\frac{E}{V_0 - E}\sin\phi\right) + \pi. \tag{38}$$

These equations are equivalent to the Fresnel formulae in optics. Note that $\cos\theta_t \leq 0$ so that $T \geq 0$ as it should. The transmission probability is plotted in Figure 5.

The transmission coefficient vanishes beyond a certain critical angle ϕ_c, which is is defined as $\sin\phi_c = (V_0 - E)/E$ (see Figs. 5 and 9). Beyond this angle, an evanescent wave is created in zone 2 and a total reflection is observed. A critical angle only occurs when $V_0/2 < E$, otherwise the conditions to have an evanescent wave $\frac{E}{V_0-E}\sin\phi > 1$ and $\frac{E}{V_0-E}\sin\phi < -1$ are never satisfied. This is similar to the optical phenomenon of total internal reflection. For instance if a light beam goes from a glass-like medium with an index n_1 to an air-like medium of index $n_2 < n_1$ then using the Snell-Descartes law $n_1 \sin\theta_1 = n_2 \sin\theta_2$, there exists a refracted beam only if the incident angle θ_1 is smaller than a critical angle $\theta_c = \arcsin(n_2/n_1)$.

If the electron arrives at normal incidence ($\phi = 0$) the probability to go through is 1:

$$T(\phi = 0) = 1. \tag{39}$$

[6] The reflection coefficient R is always equal to $|r|^2$, whereas the transmission coefficient T is not necessarily given by $|t|^2$. In the present case of the potential step $T = -|t|^2 \frac{\cos\theta_t}{\cos\phi} \neq |t|^2$. There is a mistake precisely on that point in [31]. As an illustration of the fact that T is generally not given by $|t|^2$, we consider an extreme example where the transmission probability vanishes $T = 0$ although $t \neq 0$. If in zone 2, the kinetic energy vanishes $E_{\rm kin} = E - V_0 = 0$, there is an evanescent wave when $\phi \neq 0$. Then using equation (9) and (15), we can show that $r = \exp(i2\phi)$ and therefore $T = 1 - |r|^2 = 0$, while $t = 1 + \exp(i2\phi) \neq 0$.

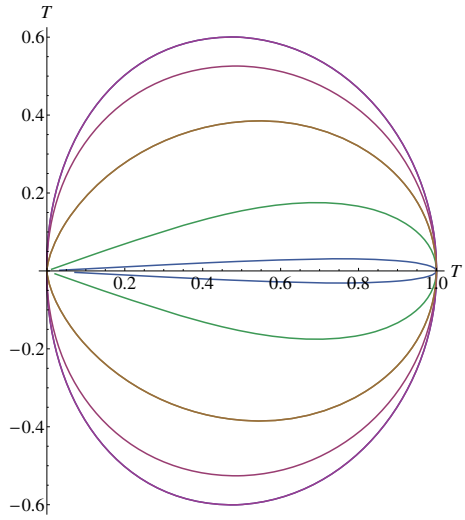

Fig. 5. Polar plot of the transmission probability $T(\phi)$ for the potential step (values of T are shown on all axis) for several dimensionless energies $\varepsilon \equiv E/V_0$ between 0 and 1 and with the incident angle ϕ running from $-\pi/2$ to $\pi/2$: $\varepsilon = 0$ (blue), $\varepsilon = 0.25$ (purple), $\varepsilon = 0.5$ (beige), $\varepsilon = 0.75$ (green) and $\varepsilon = 0.95$ (black). Note that for $\varepsilon = 0.75$ there is a critical angle above which T is strictly equal to zero.

This is due to the "absence of backscattering" discussed previously (see Sect. 2.7.2 and Refs. [25,26]) and is a consequence of the pseudo-spin conservation of the massless Dirac electron. This (at first) surprising result is most often referred to as the "Klein tunnel effect" although it is not a genuine tunnel effect in the quantum mechanical sense. Indeed it involves no classically forbidden region and no evanescent wave. It is a consequence of (1) the existence of negative kinetic energy states (valence band) in the step, that match the positive kinetic energy states (conduction band) outside the step and (2) of the conservation of pseudo-spin which permits the transition. This second point is quite important. The chirality factor acts as a selection rule. Indeed the square of the scalar product between the incoming and the transmitted bispinors is $[1+\alpha\alpha'\cos(\theta_t-\phi)]/2 = 1$ as $\alpha = +1 = -\alpha'$, $\theta_t = \pi$ when $\phi = 0$. However, it is not because states are available in the step at the matching energy that the transition will necessarily happen. The case of the bilayer graphene (with its massive chiral electrons) is illuminating in this respect [9]. In a graphene bilayer, the carriers are also described by a bispinorial wavefunction, but with a Berry phase of 2π (instead of π for the monolayer). The low energy effective Hamiltonian is

$$\hat{H}_{\text{bilayer}} = -\frac{\hbar^2}{2m^*}[(k_x^2 - k_y^2)\hat{\sigma}_x + 2k_xk_y\hat{\sigma}_y] \qquad (40)$$

for a single valley, where m^* is the effective mass of the carriers. As the band structure is also that of a gapless semiconductor – although with parabolic bands

$$E = \pm(\hbar\boldsymbol{k})^2/(2m^*)$$

– there are also states of negative kinetic energy available in the step. Here, however, the pseudo-spin conservation forbids the interband transition at normal incidence $T(\phi = 0) = 0$. Indeed the chirality factor[7] in this case is $[1+\alpha\alpha'\cos 2(\theta_t-\phi)]/2 = 0$ as $\alpha = +1 = -\alpha'$, $\theta_t = \pi$ when $\phi = 0$. The 1D case is studied in Appendix.

Some special set of energy E and incidence angle ϕ are worth mentioning. For instance, if $E = V_0/2$ one has (see also [10]):

$$T = \cos^2\phi = 1 - (k_y/k_F)^2 \qquad (41)$$

and if $E \ll V_0$ (because $\theta_t \to \pi$):

$$T = \frac{2\cos\phi}{1+\cos\phi}. \qquad (42)$$

These two cases are quite interesting (see Fig. 5). There is no critical angle, and the transmission is always quite large unless ϕ becomes really close to $\pm\pi/2$. There is a slight preference for normal incidence but no true collimation effect. This will later be compared to the case of a smooth step.

3.2 Energy above a sharp step ($V_0 < E$)

This corresponds to a nn' junction. For $x < 0$ the kinetic energy is E and for $x > 0$ the kinetic energy is $E - V_0 > 0$. Here we will consider both $V_0 > 0$ and $V_0 < 0$. The wavefunctions are:

$$\psi_1 = e^{ik_y y}\left[e^{ik_x x}\begin{pmatrix}1\\+e^{i\phi}\end{pmatrix} + e^{-ik_x x}\begin{pmatrix}1\\+e^{i(\pi-\phi)}\end{pmatrix}\right] \qquad (43)$$

$$\psi_2 = te^{ik_y y}e^{ik'_x x}\begin{pmatrix}1\\+e^{i\theta_t}\end{pmatrix} \qquad (44)$$

and the Snell-Descartes relation reads:

$$E\sin\phi = (E - V_0)\sin\theta_t. \qquad (45)$$

This leads to a new system of equations that can be solved to give:

$$r = \frac{e^{i\phi} - e^{i\theta_t}}{e^{-i\phi} + e^{i\theta_t}} \qquad (46)$$

$$t = \frac{e^{-i\phi} + e^{i\phi}}{e^{-i\phi} + e^{i\theta_t}} \qquad (47)$$

and one eventually obtains

$$T = |t|^2\frac{\cos\theta_t}{\cos\phi} = \frac{\cos\phi\cos\theta_t}{\cos^2\left(\frac{\phi+\theta_t}{2}\right)} \qquad (48)$$

where:

$$\theta_t = \arcsin\left(\frac{E}{E - V_0}\sin\phi\right). \qquad (49)$$

When $V_0 > 0$, this case corresponds to refraction indices $n_1 > 0$ and $n_2 > 0$ (equivalent to usual optical materials:

[7] Note the factor of two difference in the cosine. This is a consequence of the Berry phase being 2π rather than π.

the refraction is normal) with $n_1 > n_2$, so that there is also a critical angle given by $\sin\phi_c = (E - V_0)/E$. This is typically similar to a light beam going from glass to air. In classical mechanics, there is a similar phenomenon. Consider a non-relativistic particle of mass m and energy $E = \boldsymbol{p}^2/(2m)$ incident on a potential step of energy V_0 such that $V_0 < E$. The conservation of energy $p^2/(2m) = p'^2/(2m) + V_0$ and that of parallel momentum $p'_y = p_y$ imply that $p'^2_x/(2m) = p_x^2/(2m) - V_0$. The particle will therefore be reflected if $p'^2_x < 0$ because a negative kinetic energy is classically forbidden. This defines a critical angle of incidence ϕ_c given by $\sin\phi_c = \sqrt{(E - V_0)/E}$, where the angle ϕ is defined by $\tan\phi = p_y/p_x$. We note that the non-relativistic refraction index $n \propto \sqrt{E_{\rm kin}} \propto |\boldsymbol{p}|$ differs from the ultra-relativistic one of graphene $n \propto E_{\rm kin} = \alpha|\boldsymbol{k}|$.

When $V_0 < 0$, this case corresponds to refraction indices $n_1 > 0$ and $n_2 > 0$ with $n_1 < n_2$, so that there is no critical angle. This is typically similar to a light beam going from air to glass.

Using the Schrödinger equation (parabolic band approximation), the fact that a particle with an energy above a potential step ($E > 0 > V_0$) and with an incident velocity in the same direction as the step force ($F = -\nabla V$) can be reflected is known as a "quantum reflection", because it can not be understood from a classical perspective. It is particularly spectacular for perpendicular incidence ($\phi = 0$) and low energy $E \ll |V_0|$ where the transmission probability vanishes $T \to 0$. In the present case of a massless Dirac electron, quantum reflection is absent as $T(\phi = 0) = 1$ for any energy $E \geq 0$. This is again a consequence of the absence of backscattering.

3.3 Smooth potential step

We now turn to the case of a smooth potential step, which was recently considered by Cheianov and Falko in the context of a *np* junction in graphene [10]. Take a smooth potential step of height V_0, which occurs over a distance $2w$ (Fig. 6). Smoothness roughly means $\lambda_F \ll w$ (below, we discuss a refined criterion). The potential is taken to be $V(x) = \mathrm{sign}(x)V_0/2$ when $|x| > w$ and $V(x) = Fx$ when $|x| < w$, with $F = V_0/(2w)$. We consider a symetric situation: that of an incoming massless Dirac electron with an energy which is half that of the step. This energy is here $E = E_F = 0$ as a result of the shift in the zero of energy – indeed $V(x < -w) = -V_0/2$. The electron has a wavevector $(k_x, k_y) = k_F(\cos\phi, \sin\phi)$ where $k_F = V_0/2$. A normally incident electron $k_y = 0$ is perfectly transmitted as a consequence of the absence of backscattering. We focus on the case $k_y \neq 0$ which gives rise to a classically forbidden zone close to $V(x) = E$ (i.e. $x = 0$). It can be found from the conservation of energy $\sqrt{k_x(x)^2 + k_y^2} + Fx = E = 0$ and the requirement that $k_x(x)^2 < 0$. This defines the region $|x| < l_c \equiv k_y/F$. The size of the classically forbidden zone is $2l_c = 2w\sin\phi$. An electron with $k_y \neq 0$ that wishes to go through the step has to tunnel via evanescent waves to the other side across the classically forbidden zone. In the semiclassical approximation, the probability amplitude to tunnel is given by $A \approx e^{iS}$ where $S = \int_{-l_c}^{+l_c} dx\, k_x(x)$ is the (reduced) action, which is imaginary when $k_x(x) = i|k_x(x)| = i\sqrt{k_y^2 - (Fx)^2}$. The tunneling probability is then $T = |A|^2$. The typical $k_x(x)$ is $k_x(0) = ik_y$, therefore $S \sim ik_y \times 2l_c$ and $T \sim e^{-4k_y l_c}$. More precisely, $S = ik_y l_c \int_{-1}^{1} du\sqrt{1 - u^2} = i\pi k_y l_c/2$ and the probability is [10]:

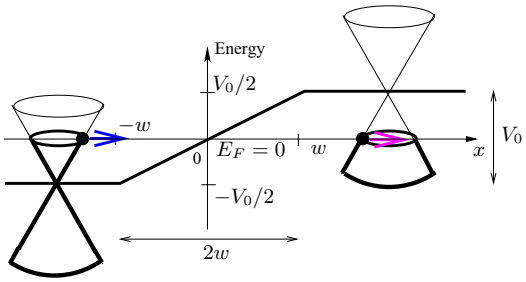

Fig. 6. Band structure across a smooth *np* junction. The potential height is V_0 and its width is $2w$. The energy of the incoming electron (Fermi energy) is half that of the potential step. The zero of energy is chosen to coincide with the Fermi level. Arrows indicate the direction of motion before (blue) and after (pink) the step.

$$T(\phi) \approx e^{-\pi k_y l_c} = e^{-\pi k_y^2/F} = e^{-\pi k_F w \sin^2\phi}. \qquad (50)$$

This result is valid for a smooth step and for incidence angles ϕ not too close to $\pi/2$. It satisfies $T(0) = 1$ and $T(\phi) \approx 1$ for incidence angles such that $|\phi| \ll \phi_0 \equiv \sqrt{F/\pi k_F^2} = 1/\sqrt{\pi k_F w}$ – where ϕ_0 is called the collimation angle –, and then rapidly goes to zero for oblique incidence $|\phi| > \phi_0$. This shows that a single *np* junction has a collimation effect as it focuses the electronic flow by allowing the transmission of only the trajectories that are close to normal incidence [31]. This result should be compared to $T = \cos^2\phi$ found previously in the case of a sharp step (see Fig. 7). Apart from small incidence angles, chirality seems not to play an important role here. This tunneling is similar to interband tunneling in a Zener diode, see e.g. [33]. In a semiconductor, one can have a junction between an electron-doped and a hole-doped region (a so-called *np* junction). If the voltage difference across the tunnel junction is strong enough, it is possible for electrons to tunnel from the conduction to the valence band across the junction. The only difference here is that the semiconductor is 2D, gapless and the bands are linearly dispersing.

The transition between the abrupt ($w \to 0$) and smooth ($w \to \infty$) steps limit is treated in [34]. Actually, a step is considered smooth when the semiclassical approximation is valid. This happens when the typical tunneling action is large $|S| \sim k_x(0)l_c = k_y w\sin\phi = k_F w\sin^2\phi \gg 1$. The smoothness criterion is therefore $k_F w\sin^2\phi \gg 1$. It not only depends on $k_F w$ but also on the incidence angle ϕ. Close to normal incidence, any step becomes sharp (see Fig. 1b in Ref. [34]). If $k_F w < 1$, the step is sharp at any incidence angle. If $k_F w > 1$, the step is sharp close to

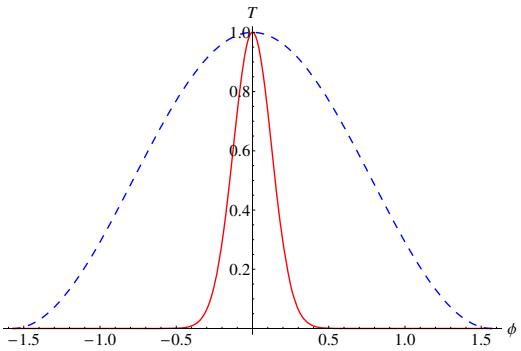

Fig. 7. Transmission probability $T(\phi)$ across a potentiel step for an energy which half that of the barrier. T (on the y axis) is plotted as a function of the incidence angle ϕ (on the x axis) between $-\pi/2$ and $\pi/2$ for a sharp (dashed blue, $T = \cos^2\phi$) and a smooth step (red, $T = e^{-\pi k_F w \sin^2\phi}$ with $k_F w = 10$). The collimation effect is clearly seen in the smooth step case, with a characteristic angle $\phi_0 = 1/\sqrt{\pi k_F w} \approx 0.2$.

normal incidence and smooth close to grazing incidence. In the "sharp step angular region" ($|\phi| \ll 1/\sqrt{\pi k_F w}$), the transmission is high and corresponds to the absence of backscattering; whereas in the "smooth step angular region" ($|\phi| > 1/\sqrt{\pi k_F w}$), transmission is exponentially suppressed and occurs via evanescent wave inter-band tunneling. The signature of chirality for the smooth step is therefore in the collimation effect: only electrons sufficiently close to normal incidence are transmitted across the junction.

When the energy of the incoming electron is not half that of the barrier, the transmission probability becomes [12]:

$$T(\phi) \approx \exp\left(-\pi \frac{2k_{F1}^2}{k_{F2}+k_{F1}} w \sin^2\phi\right) \tag{51}$$

where k_{F1} (resp. k_{F2}) is the Fermi wavevector in the zone 1 (resp. zone 2). The symetric case considered above corresponds to $k_{F1} = k_{F2} = k_F$.

4 Potential barrier

Let us now consider a square potential barrier [9], see also [35]. We distinguish three zones: zone 1 for $x < 0$, where the potential is equal to 0; zone 2 for $0 < x < d$, where the potential is equal to V_0; and zone 3 for $x > d$, where the potential is again 0. And study two cases: $0 < E < V_0$ (coresponding to a *npn* junction) and $E > V_0 > 0$ ($nn'n$ junction).

4.1 Energy below the barrier ($0 < E < V_0$)

This corresponds to a *npn* junction in graphene. Using the equations of Section 2 the wave functions can be written

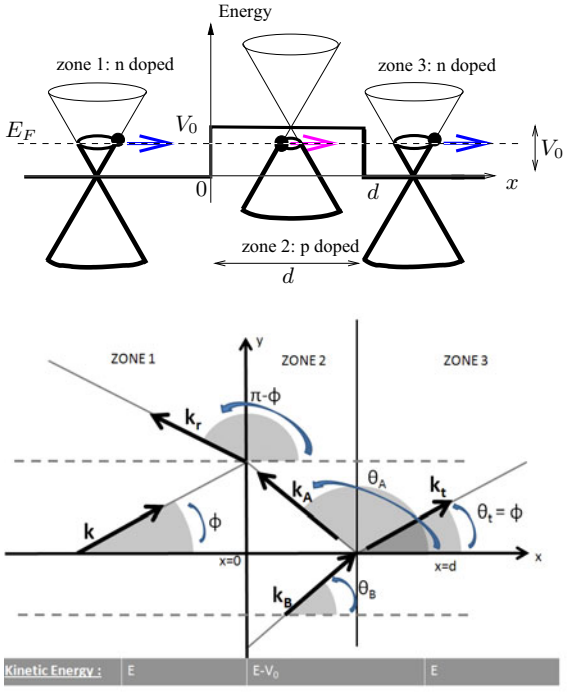

Fig. 8. Top: band structure across a sharp *npn* junction. An electron of energy $0 < E < V_0$ is incident from the left on a square potential barrier of height V_0 and width d. Note the position of the Dirac cone tips in the three zones. Bottom: definition of the angles and the wavevectors in the three zones: incident $\boldsymbol{k} = (k_x, k_y) = E(\cos\phi, \sin\phi)$, reflected $\boldsymbol{k_r} = (-k_x, k_y) = E(\cos(\pi-\phi), \sin(\pi-\phi))$, transmitted inside the barrier $\boldsymbol{k_A} = (k'_x, k_y) = -(E-V_0)(\cos\theta_A, \sin\theta_A)$, reflected inside the barrier $\boldsymbol{k_B} = (-k'_x, k_y) = -(E-V_0)(\cos\theta_B, \sin\theta_B)$ and transmitted $\boldsymbol{k_t} = \boldsymbol{k}$.

in the three zones (see Fig. 8):

$$\psi_1 = e^{ik_y y}\left[e^{ik_x x}\begin{pmatrix}1\\+e^{i\phi}\end{pmatrix} + re^{-ik_x x}\begin{pmatrix}1\\-e^{-i\phi}\end{pmatrix}\right] \tag{52}$$

$$\psi_2 = e^{ik_y y}\left[Ae^{ik'_x x}\begin{pmatrix}1\\-e^{i\theta_A}\end{pmatrix} + Be^{-ik'_x x}\begin{pmatrix}1\\e^{-i\theta_A}\end{pmatrix}\right] \tag{53}$$

$$\psi_3 = te^{ik_y y}e^{ik_x x}\begin{pmatrix}1\\e^{i\phi}\end{pmatrix}. \tag{54}$$

With the continuity of the spinors in $x = 0$ and $x = d$, the following system is obtained:

$$1 = -r + A + B \tag{55}$$

$$e^{i\phi} = re^{-i\phi} - Ae^{i\theta_A} + Be^{-i\theta_A} \tag{56}$$

$$0 = -te^{ik_x d} + Ae^{ik'_x d} + Be^{-ik'_x d} \tag{57}$$

$$0 = -te^{i\phi}e^{ik_x d} - Ae^{i\theta_A}e^{ik'_x d} + Be^{-i\theta_A}e^{-ik'_x d} \tag{58}$$

where A, B, r and t are complex amplitudes to be determined. The easiest method to solve this system is by

substitution and only r is worth computing [9]:

$$r = -2e^{i\phi}\sin(k'_x d) \times \frac{\sin\phi + \sin\theta_A}{e^{-ik'_x d}\cos(\phi+\theta_A) + e^{ik'_x d}\cos(\phi-\theta_A) + 2i\sin(k'_x d)}. \quad (59)$$

The transmission coefficient follows from $T = 1 - |r|^2$:

$$T = \frac{\cos^2\phi\cos^2\theta_A}{\cos^2\phi\cos^2\theta_A\cos^2(k'_x d) + \sin^2(k'_x d)[1+\sin\theta_A\sin\phi]^2} \quad (60)$$

where $k'_x d = -2\pi l\sqrt{1-2\varepsilon+\varepsilon^2\cos^2\phi}$ with the dimensionless barrier width $l \equiv V_0 d/(2\pi\hbar v_F) = V_0 d/(2\pi)$ and the dimensionless energy $\varepsilon \equiv E/V_0$. Naturally, from the conservation of k_y we can obtained the Snell-Descartes law:

$$E\sin\phi = -(E - V_0)\sin\theta_A. \quad (61)$$

Several cases are worth investigating.

4.1.1 Low energy ($E \ll V_0$)

The incoming electron has an tiny energy compared to V_0 and the transmission coefficient takes a simpler form [9]:

$$T = \frac{\cos^2\phi}{1 - \cos^2(k'_x d)\sin^2\phi}. \quad (62)$$

4.1.2 Grazing energy ($E \to V_0^-$)

Here, the electron arrives exactly with the energy of the barrier. The transmission is entirely via evanescent waves (except exactly at $\phi = 0$). When $E_{\rm kin} = 0$, $k'_x = ik_y$ and therefore $1/\cos\theta_A = |E_{\rm kin}|/k'_x = 0$ and $\tan\theta_A = k_y/k'_x = -i$. Therefore equation (60) becomes:

$$T = \frac{\cos^2\phi}{\cosh^2(k_y d) - \sin^2\phi} \quad (63)$$

where we used that

$$\cos^2(ik_y d) = \cosh^2(k_y d) \text{ and } \sin^2(ik_y d) = -\sinh^2(k_y d).$$

Note that it is not obvious a priori that a formula obtained for oscillating waves remains valid in a regime of evanescent waves.

4.1.3 Normal incidence ($\phi = 0$)

If the incident angle is zero (the angle is taken from the x-axis), the transmission coefficient is exactly equal to 1 regardless of the length d and the (energy) height V_0 of the barrier. This perfect transmission at normal incidence is again due to the conservation of the pseudo-spin leading to the absence of backscattering (see Sect. 2.7). In particular, it is not an interference effect between the two interfaces at $x = 0$ and $x = d$. For such an effect, see Section 4.1.5 on Fabry-Pérot resonances.

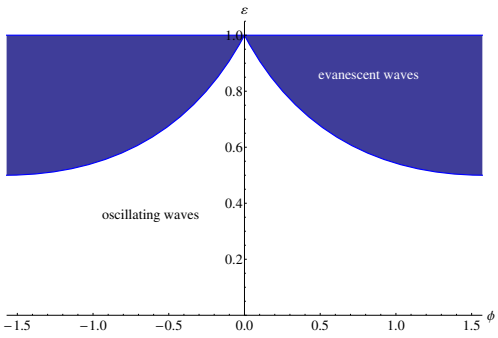

Fig. 9. "Phase diagram" for the wave nature inside the barrier plotted in the (ϕ, ε) plane. On the y-axis is the dimensionless energy $\varepsilon \equiv E/V_0$, on the x-axis is the incident angle ϕ running from $-\pi/2$ to $\pi/2$. The white area is the zone of oscillating waves (classically allowed region; possibility of resonances), the blue area is the zone of evanescent waves (classically forbidden; possibility of true tunnel effect via an evanescent wave). The two regions are separated by the critical angle line ϕ_c such that $\sin\phi_c = (1-\varepsilon)/\varepsilon$.

4.1.4 Critical angle ($1/2 < \varepsilon < 1$)

As with the potential step, once a critical angle defined as $\sin\phi_c = (V_0 - E)/E$ is reached, an evanescent wave is present in the zone 2. But contrary to what happened with the step, there is no total reflection. Indeed, the existence of a second discontinuity between the zone 2 and the zone 3 allows the wave to be transmitted through the barrier with a reduced amplitude, just like in the Schrödinger tunnel effect: passing through is classically forbidden but quantum mechanically permitted via an evanescent wave. This is therefore a genuine tunnel effect. The condition to have an evanescent wave is that the wavevector projection along x in zone 2 is purely imaginary: ${k'_x}^2 < 0$ [8]. As ${k'_x}^2 d^2 = (2\pi l)^2(1 - 2\varepsilon + \varepsilon^2\cos\phi)$, the condition to have an evanescent wave is:

$$1 - 2\varepsilon + \varepsilon^2\cos\phi < 0. \quad (64)$$

There are no evanescent waves for an electron with an energy below $V_0/2$. The critical angle is plotted in Figure 9 in a kind of "phase diagram".

4.1.5 Fabry-Pérot resonances ($\phi \neq 0$)

We now restrict to oblique incidence ($\phi \neq 0$) and consider multiple interferences effects. A potential barrier can be seen as a double interface (at $x = 0$ and $x = d$) and as the analog of a well-known optical system: a Fabry-Pérot interferometer. The cavity is the region inside the

[8] Note that the condition for having an evanescent wave in the barrier is the same as that for total reflection on the potential step and defines the critical angle. As ϕ runs between $-\pi/2$ to $\pi/2$, the function $\sin\phi$ increases with ϕ and $\cos\phi \geq 0$. Therefore $\phi > \phi_c$ with $\sin\phi_c = \frac{1-\varepsilon}{\varepsilon} \Leftrightarrow \sin\phi > \sin\phi_c = \frac{1-\varepsilon}{\varepsilon}$, hence $\varepsilon^2\sin^2\phi > (1-\varepsilon)^2 = 1 + \varepsilon^2 - 2\varepsilon \Leftrightarrow 1 - 2\varepsilon + \varepsilon^2\cos\phi < 0$, which is precisely the same as $k'^2_x < 0$.

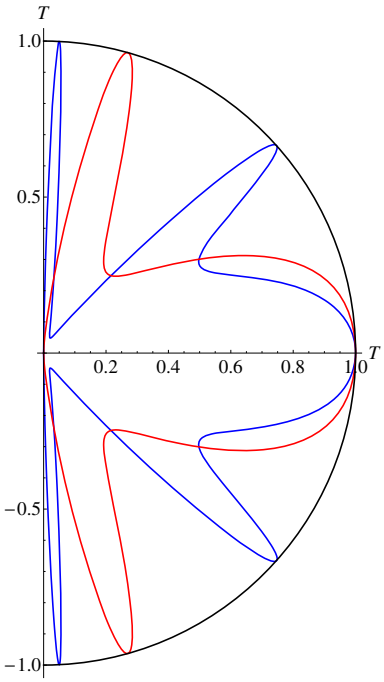

Fig. 10. Polar plot of the transmission coefficient $T(\phi)$ for the potential barrier at fixed energy ε and width l. The two sets of parameters are the same as in [9] namely: ($\varepsilon = 0.41519$, $l = 4.85$, blue) and ($\varepsilon = 0.291038$, $l = 6.91$, red). The petal structure is clearly seen and correspond to Fabry-Pérot resonances. Note that $T(0) = 1$ as a consequence of pseudo-spin conservation and independently of ε and l. The black line indicates unit transmission.

barrier, which can accommodate oscillating waves – especially at $\varepsilon < 1/2$, see Figure 9. Accordingly, the incoming wave might interfere with itself between the two interfaces (at $x = 0$ and $x = d$) in zone 2. If the waves interfere constructively transmission resonances will occur where $T(\phi \neq 0) = 1$. The condition of such resonances[9] – also known as tunneling resonances – is [9]:

$$k'_x d = \pi \times \text{integer} \tag{65}$$

which is just the condition that a half-integer ($\mathbb{N}/2$) number of wavelengths ($2\pi/k'_x$) along x fits in the cavity (i.e. inside the barrier) of size d: (integer/2)$(2\pi/k'_x) = d$. As $k'_x d = -2\pi l\sqrt{1 - 2\varepsilon + \varepsilon^2 \cos^2\phi}$, the resonance condition involves the energy ε, the length of the barrier l and the angle ϕ and reads:

$$2l\sqrt{1 - 2\varepsilon + \varepsilon^2 \cos^2\phi} = \text{integer}. \tag{66}$$

It defines specific angles $\phi_n \neq 0$ such that $T(\phi_n) = 1$. These Fabry-Pérot resonances are responsible for the petal-like shape of $T(\phi)$ when plotted as a function of the incidence angle ϕ at fixed energy ε and barrier width l (see Figs. 10 and 11, and Ref. [9]).

[9] Note that the backreflections phases accumulated at the two interfaces have opposite signs, their sum vanishes and therefore do not appear in the resonance condition [36].

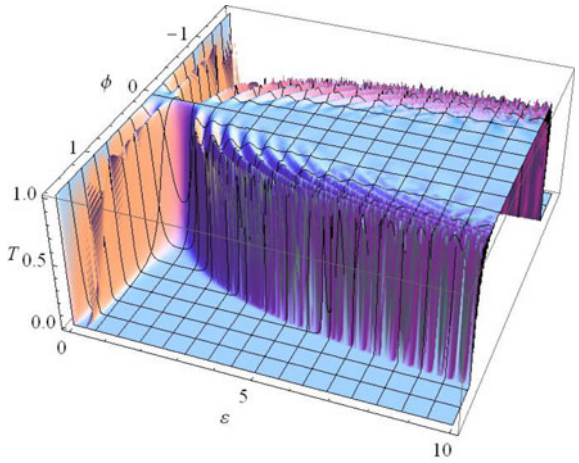

Fig. 11. Plot of the transmission probability T as a function of the incident angle ϕ and the dimensionless energy $\varepsilon \equiv E/V_0$ for a fixed dimensionless width of the barrier $l = 1$. The energy ε varies between 0 and 10 and the angle ϕ between $-\pi/2$ and $+\pi/2$. Fabry-Pérot resonances are clearly visible.

4.2 Energy above the barrier ($E > V_0 > 0$)

We now focus on the situation where an electron is incident with an energy larger than the one of the barrier (corresponding to a $nn'n$ junction). After proceeding with the same kind of computation as for the other case, we obtain a transmission coefficient which has the same expression as (60) and (61) with the replacement $\theta_A \to -\theta_A$. Within this energy range, most of the properties of the transmission coefficient are retrieved. In the high energy limit ($E \gg V_0 > 0$) limit, we find the transmission probability:

$$T = \frac{\cos^2\phi}{1 - \cos^2 k'_x d \sin^2\phi}. \tag{67}$$

4.3 Grazing energy ($E = V_0 > 0$)

Both limits $E \to {V_0}^{\pm}$ have the same common value, therefore $T(E = V_0) = T(E = {V_0}^{\pm})$:

$$T = \frac{\cos^2\phi}{\cosh^2(k_y d) - \sin^2\phi}$$

This result plays a key role in the calculation of the two-terminal conductance of a ballistic undoped graphene sheet using the Landauer formula (see [37] and [38]). The reservoirs are assumed to be made of doped graphene and the sample is undoped. In order to ensure that the reservoirs conduct much better than the undoped graphene sheet, one takes the limit of a very large doping of the reservoirs (many transverse channels in the reservoirs): this is equivalent to $\sin\phi \to 0$. In this limit ($\phi \to 0$), the transmission coefficient becomes:

$$T \approx \frac{1}{\cosh^2(k_y d)}. \tag{68}$$

This corresponds to a genuine tunnel effect through the sample (except at $\phi = 0$). Indeed, when $k_y d \gg 1$,

$T \approx 4\exp(-2k_y d) \ll 1$, which is of the expected semi-classical form with a tunneling probability proportional to $\exp(-2S_i)$, where $S_i = k_y d$ is the imaginary time action for the classical path inside the barrier.

To conclude this section on the potential barrier, we mention that the case of a smooth (trapezoidal) barrier has been treated in [39]. See in particular the discussion of Fabry-Pérot resonances.

5 Experiments

Below we describe the current status of transport experiments designed at observing the Klein tunnel effect in graphene and rely mainly on the following papers [12–15], but mention also other relevant experiments [40–43]. For reading convenience, in this section, we restore the units of $\hbar$ and v_F.

5.1 Backgate and topgate

Graphene samples are usually equiped with a backgate that allows one to electrically control the doping of the sheet through an electric field effect (similar to a capacitor) [44]. In exfoliated samples, the backgate is usually made of doped silicon and separated from the graphene sheet by ∼300 nm of silicon dioxide (dielectric). Electrostatic potential steps and barriers can be made by using an additional topgate. The simultaneous use of a backgate and a topgate allows one to control independently the energy of incoming electrons (E_F) and the step/barrier height (V_0). The distance between the topgate and the graphene sheet roughly gives the step size $2w$. Steps made in this way are smooth on the lattice scale ($w \gg a$, as an example $2w \sim 80$ nm [12]) and until recently also smooth on the Fermi wavelength scale ($w > 1/k_F$, typically $1/k_F \sim 10$ nm). Sharp steps ($w < 1/k_F$) should soon become available thanks to rapid progress in fabrication[10]. The typical barrier width d is in between 100 nm and 1 μm.

Transport measurement are performed on these systems, in which the two-terminal resistance is measured as a function of the backgate and topgate voltages. Roughly speaking, the backgate controls the Fermi energy and the topgate sets the barrier properties (height V_0, width d and step size $2w$). One may in addition apply a magnetic field in order to measure the magneto-resistance.

5.2 Ballistic versus diffusive regime

The samples are usually small: the distance L between two measuring contacts is typical less than 1 μm. This is done in order to be as close as possible to the ballistic regime, in which collisions on impurities can be neglected (note that our complete discussion of Klein tunneling assumed that we could neglect the effect of disorder). To know whether this is indeed the case implies to compare the mean free path l_m with the step size $2w$, the barrier width d and the sample size L. Depending on the situation, it is possible to have a sample which is, for example, globally diffusive ($l_m \ll L$), that the barrier is diffusive ($l_m \ll d$) but that each step can be described as being ballistic ($l_m \gg w$). The mean free path in a good graphene sample is typically on the order of $l_m \sim 100$ nm. The effect of disorder on a graphene np junction is discussed in [45]. These authors find that the transition between ballistic ($\beta \gg 1$) and diffusive ($\beta \ll 1$) regimes is controlled by a single dimensionless parameter $\beta \equiv |dn/dx|/n_i^{3/2}$, where dn/dx is the density gradient right at the junction and $n_i \equiv e/h\mu_m$ – where μ_m is the mobility – roughly gives the density of impurities. This prediction was confirmed experimentally [14].

Low temperature is also needed in order to have coherent propagation of the electrons (no decoherence). This corresponds to our assumption of treating the electron as ideal matter waves, rather than classical particles. The coherence length in a graphene sample is typically $L_\phi \gtrsim 1$ μm when the temperature is below 4 K.

5.3 Smooth np junctions and poor screening

Potential steps realized up to now were generally of the smooth type. However, the slope F of the potential step $V(x) \approx Fx$ right at the junction (when $V(x) = E_F$) is not properly estimated as $V_0/2w$ (as we did in Sect. 3.3). Such an estimate relies on assuming perfect screening in the graphene sheet, which is not correct. Indeed, close to the bipolar junction, screening in graphene is very poor because it corresponds to the crossing of the Dirac point where the density of states vanishes. Linear Thomas-Fermi screening would predict no screening at all, as the inverse screening radius vanishes. It is however possible to study non-linear screening in this regime. This was done by Zhang and Fogler for a ballistic np junction [46]. They find that the slope F is strongly enhanced compared to the naive estimate $V_0/2w$ (typically by a factor of 10). This effect is important to take into account when comparing theory and experiment [14,15].

5.4 Evidences for the observation of Klein tunneling

5.4.1 Resistance of a smooth ballistic np junction

The first experiments designed at observing Klein tunneling in graphene all measured the resistance across a npn junction as a function of topgate and backgate voltages [12–14]. Because of the presence of disorder, the resistance of the barrier was found to be correctly described as the sum of the resistance of two smooth np junctions (in series). Each np junction was in the ballistic regime but

[10] Reaching small k_F values is limited by the presence of so-called electron-hole puddles close to the Dirac point in a graphene sheet. These inhomogeneities mean that locally the Fermi wavevector is never really zero but has a finite minimal value. The cleanest suspended samples correspond to $1/k_F \sim 100$ nm.

not the whole barrier. As the momentum of an electron is not conserved during its motion between the two interfaces, cavity type resonances are not possible, see e.g. [47]. We therefore consider these experiments as testing the resistance R across a smooth step (np junction) rather than a barrier.

In order to set the stage, we give typical values of relevant quantities. The barrier height $V_0 \sim 0.1$ eV, width $d \sim 300$ nm and step size $2w \sim 100$ nm; the Fermi wavelength $1/k_F \sim 10$ nm such that $k_F w \sim 5$ (smooth step); the mobility $\mu_m \sim 1000{-}10\,000$ cm^2/V s, the mean free path $l_m \sim 30{-}100$ nm and the length between measuring contacts $L \sim 1.3{-}5$ μm.

These measurements probe the average transmission across the junction. Indeed, the two terminal conductance $G = 1/R$ is given by the Landauer formula

$$G_{np} = 4\frac{e^2}{h}\sum_{ch.} T_{ch.} \approx 4\frac{e^2}{h}\int_{-k_F}^{k_F}\frac{dk_y}{2\pi/W}T(k_y) \qquad (69)$$

where the sum is over transverse channels labelled by $k_y = k_F \sin\phi$ and with transmission probability $T(k_y)$, W is the sample width (not to be confused with the step size w) and the factor 4 accounts for valley and spin degeneracy in graphene.

As an example, we consider a symmetric np junction: the Fermi energy is at half the potential step. On the one hand for a smooth step of potential slope F at the junction, the transmission is $T(k_y) = e^{-\pi\hbar v_F k_y^2/F}$ (see Sect. 3.3) and therefore [10]:

$$G_{np}^{\text{smooth}} = \frac{2e^2}{\pi h}W\sqrt{\frac{F}{\hbar v_F}}. \qquad (70)$$

On the other hand, for a sharp symmetric step, the transmission is $T = \cos^2\phi = 1 - (k_y/k_F)^2$ (see Sect. 3.1) and therefore the conductance is:

$$G_{np}^{\text{sharp}} = \frac{8e^2}{3h}\frac{k_F W}{\pi}. \qquad (71)$$

For comparison, when there is no step, the transmission is perfect $T(k_y) = 1$ and the conductance is

$$G_{\text{no step}} = 4\frac{e^2}{h}\frac{k_F W}{\pi}. \qquad (72)$$

As $G_{np}^{\text{sharp}} = 2G_{\text{no step}}/3 \gg G_{np}^{\text{smooth}}$, we conclude that the sharp np junction is almost transparent, while the smooth np junction is highly resistive and only lets the electrons close to normal incidence through (collimation effect). Note that from the measurement of G_{np}^{smooth} and $G_{\text{no step}}$ it is possible to estimate the collimation angle as $G_{np}^{\text{smooth}}/G_{\text{no step}} \sim \phi_0/2$.

The resistance measured across smooth np junctions as a function of the topgate voltage (controlling the barrier properties) was found [13,14] in agreement with theory provided the ballistic regime is reached ($\beta \gg 1$) [45] and the poor screening in graphene close to the junction is acounted for [46]. Quite counter-intuitively[11], the resistance across a smooth junction was measured to *exceed* that predicted in a purely diffusive model (i.e. excluding chirality effects) but to agree with the ballistic prediction. The signature of Klein tunneling was precisely found in this collimation effect that only allows electrons close to normal incidence to go through the smooth junction.

Although the average transmission was found to agree with the prediction of Klein tunneling across a smooth np junction, the angular dependence of the transmission probability $T(\phi)$ was not seen. In particular, from a measurement of the average transmission, it is not possible to tell that perfect tunneling occurs at normal incidence or to precisely measure the collimation angle. A measurement of the resistance across a sharp ballistic junction would be closer to revealing perfect tunneling as its resistance is predicted to be only 3/2 times larger than in the absence of a step. In conclusion, these first experiments gave indirect evidences of Klein tunneling in graphene bipolar junctions.

5.4.2 Conductance oscillations and magneto-resistance across a ballistic npn junction

A second type of experiment was performed in order to test Klein tunneling more directly, which relied on quantum interferences between two pn interfaces. A graphene npn junction was realized with a narrow topgate such that the whole barrier was in the ballistic regime [15]. Indeed, the mean free path was estimated as $l_m \gtrsim 100$ nm larger than the barrier width $d < 100$ nm. The step of size $2w \sim 30$ nm was smooth compared to both the lattice spacing and the Fermi wavelength $1/k_F \sim 4$ nm. The mobility was $\mu_m \sim 5000$ cm^2/V s, the distance between measuring contacts $L \sim 3$ μm and the typical barrier height $V_0 \sim 0.3$ eV. Two main observations were made on this system.

First, oscillations in the conductance as a function of the top gate voltage revealed that the whole npn junction was (for the first time) in the ballistic regime. These oscillations where interpreted as interferences due to multiple reflections between the two pn interfaces (see Sect. 4.1.5 on Fabry-Pérot resonances). The topgate allows one to tune these transmission resonances and to span the interference fringes. Note that, due to perfect tunneling at normal incidence, Fabry-Pérot resonances are only possible for oblique ($\phi \neq 0$) trajectories.

[11] A widespread misconception about Klein tunneling is that it should systematically allow electrons to go through any barrier with a high probability. If this was true, it would indeed seem counter-intuitive that an experimental evidence for Klein tunneling comes from measuring an *increase* of the resistance. Note that this increase is here defined with respect to a diffusive model and not to a situation in which Klein tunneling would be simply turned off. And that the evidence for Klein tunneling in such an experiment on smooth junctions is in the collimation effect.

Second, applying a perpendicular magnetic field, resistance measurements revealed a half-period shift in these Fabry-Pérot fringes above a critical magnetic field ∼0.3 T. The interpretation is as follows [36]. Reflectionless transmission at normal incidence ($\phi = 0$) – in other words, Klein tunneling – also means that the reflection amplitude r undergoes a π phase jump when the incident angle ϕ goes from positive to negative value[12]. At zero magnetic field, two consecutive (non-normal) reflections on the two pn interfaces occur with opposite angles ϕ_1 and $\phi_2 = -\phi_1$. A weak magnetic field bends the electronic trajectories. Above a critical field, trajectory bending becomes sufficient to make the two consecutive reflections occur with the same incident angle $\phi_1 = \phi_2$. This suddenly adds π to the phase accumulated by an electron between two reflections and shifts the interference fringes by half a period. The observation of this half-period shift (see Fig. 3 in [15]) is therefore a direct evidence of perfect tunneling at normal incidence.

6 Conclusion

In conclusion, we compare Klein tunneling to the standard tunnel effect and outline what are the crucial ingredients necessary for its occurence. We also show that the phrase "Klein tunneling" has different meanings. Eventually we give indications for further reading.

The standard tunnel effect across a barrier is an intraband transition of a Schrödinger electron via evanescent waves across the classically forbidden zone (the barrier). It gives a tunneling probability at normal incidence which is roughly $T(\phi = 0) \sim e^{-2\kappa d}$ where $i\kappa$ is the typical wavevector (in the x direction, perpendicular to the barrier) inside the barrier and d is the barrier width. The probability therefore decays exponentially with the width and the energy height of the barrier (through κ).

Klein tunneling is the name given to the interband transition (say from a conduction to a valence band) across a step or barrier of a massless Dirac electron. It relies (i) on having negative kinetic energy states available in the step or barrier (matching energy of the incoming electron) and also (ii) on the pseudo-spin conservation that may allow or not the transition (roughly speaking this is a kind of selection rule given by the overlap of the bispinors outside and inside the barrier: its modulus square is the so-called chirality factor).

Depending on the precise situation Klein tunneling may refer to different physical situations and mechanisms. Here we distinguish four situations encountered in the present article (by default, it is usually the first case which is meant):

(1) At normal incidence on a potential step that is translationally invariant (along y), there is perfect interband transmission without evanescent waves:

$$T(\phi = 0) = 1.$$

This is a consequence of the absence of backscattering due to pseudo-spin $\hat{\sigma}_x$ conservation. It is not a genuine quantum tunnel effect. See Section 2.7.3.

(2) At oblique incidence on a sharp step, there can be $T < 1$ interband transmission without evanescent waves. For example, for an electron incident with an energy which is half that of the step:

$$T(\phi \neq 0) = \cos^2 \phi.$$

The chirality factor is playing a role here. See Section 3.1.

(3) At oblique incidence on a smooth step, there is interband tunneling (via evanescent waves). For example, for an electron incident with an energy which is half that of the step:

$$T(\phi \neq 0) \approx e^{-\pi \hbar v_F k_F^2 \sin^2 \phi / F}$$

where F is the potential gradient at the bipolar junction. This is a genuine quantum tunnel effect when $|\phi| > \phi_0 \equiv \sqrt{F/(\pi \hbar v_F k_F^2)}$ and chirality only plays a role close to normal incidence leading to collimation of the electrons ($|\phi| \ll \phi_0$). See Section 3.3.

(4) At oblique incidence on a square barrier, there can be Fabry-Pérot resonances. These are transmission resonances due to the multiple interferences of oscillating waves between the two interfaces:

$$T(\phi_n \neq 0) = 1 \text{ when } k'_x d = \pi n$$

see Section 4.1.5.

We end this article by giving a list of references for further reading on topics not covered in the present review. Klein tunneling has also been studied theoretically for massive Dirac electrons in "gapped graphene" [48], for massive chiral electrons in a graphene bilayer with [49] or without [9] band gap and in a deformed honeycomb lattice [50]. It was also investigated in monolayer graphene in the presence of a magnetic field [10,36,51] or a superlattice [52,53] or magnetic vector potential barriers [54]. The motion of a wavepacket through a barrier in graphene is discussed in [18].

We thank the participants of the Cargèse summer school of mesoscopics (october 2008, GDR-CNRS Physique quantique mésoscopique organised by B. Reulet, Ch. Texier and G. Montambaux), D. Jahani, M. Goerbig, G. Montambaux, Ch. Texier and especially F. Piéchon for many interesting discussions. And also M. Büttiker for encouragements and S. Guéron, B. Huard, P. Carmier and K. Loida for useful comments on the manuscript. This work was realized during the internship (June-July 2008) of P.E.A. at LPS Orsay in partial fulfillment of his master (M1) degree at the Université Paris-Sud, France.

[12] In Section 3.1, we showed that, in the case of a sharp potential step, the reflection amplitude is $r(\phi) = (e^{i\phi} + e^{i\theta_t})/(e^{i\phi} - e^{-i\theta_t})$ where $\theta_t = \pi + \arcsin(E \sin\phi/(V_0 - E))$. In the limit were $\phi = \pm\eta$ with $\eta \to 0^+$, it follows that $r(\pm\eta) \approx e^{\pm i\pi/2}\eta V_0/(2(V_0 - E))$. Therefore, there is a π phase jump (in the reflection amplitude) when the incident angle changes sign: $\mathrm{Arg}\, r(\eta) - \mathrm{Arg}\, r(-\eta) \approx \pi$ when $\eta \to 0^+$. More generally, for arbitrary η, one can show that $\mathrm{Arg}\, r(\eta) - \mathrm{Arg}\, r(-\eta) = \pi + 2[\eta + \arcsin(E \sin\eta/(V_0 - E))] = \pi + \mathcal{O}(\eta)$.

Appendix: Klein tunneling in one-dimension

As an illustration of the importance of pseudo-spin conservation, we consider Klein tunneling in 1D and study two toy-model Hamiltonians. First consider the following massless Dirac Hamiltonian – which we call the "1D monolayer":

$$\hat{H}_m = k_x \hat{\sigma}_x + V(x)\hat{1} \tag{A.1}$$

with $\hbar v_F \equiv 1$ where v_F is the Fermi velocity. The pseudo-spin is conserved as $[\hat{\sigma}_x, \hat{H}_m] = 0$, and thus also the velocity operator $\hat{v}_x = -i[x, \hat{H}_m] = \hat{\sigma}_x$ is a conserved quantity[13]. If the electron is initially in a velocity eigenstate (say such that $v_x = +1$), then $\langle \hat{v}_x(t) \rangle = +1$ at any $t > 0$. Therefore the motion of the electron in the presence of the potential is exactly the same as in its absence (the motion is not even delayed). This is a strong consequence of the absence of backscattering.

To understand the physical meaning of the pseudo-spin, we consider the case when the potential is absent. An eigenstate of the Hamiltonian is:

$$\psi_{k_x,\sigma_x}(x) = \frac{1}{\sqrt{2}} \begin{pmatrix} 1 \\ \sigma_x \end{pmatrix} e^{i\sigma_x k_x x} \tag{A.2}$$

where k_x is the momentum, $E_{\text{kin}} = \text{sign}(E_{\text{kin}})|k_x|$ is the energy and $\sigma_x = \pm 1$ is the eigenvalue of the pseudo-spin $\hat{\sigma}_x$. The latter can also be written as $\sigma_x = \text{sign}(k_x)\text{sign}(E_{\text{kin}})$ or $\sigma_x = E_{\text{kin}}/k_x$ and is therefore the direction of motion ($+1$ for right movers and -1 for left movers). If an electron is initially a right mover, it will remain so even if it encounters regions of arbitrary non-zero potential (see top of Fig. 12).

In the presence of the potential, it is also possible to find the eigenstates of the Hamiltonian (A.1), see [55]. Performing a unitary transformation the Hamiltonian can be written as $\tilde{H}_m = k_x \hat{\sigma}_z + V(x)\hat{1}$. The eigenvalue equation decouples in two equations $\mp i d\psi_\pm/dx = [E - V(x)]\psi_\pm$, which are easily solved to give the following eigenvectors

$$\psi_{E,\sigma_x}(x) \sim \frac{1}{\sqrt{2}} \begin{pmatrix} 1 \\ \sigma_x \end{pmatrix} e^{i\sigma_x \int^x dx'[E - V(x')]} \tag{A.3}$$

at any eigenenergy E. Each energy level is doubly degenerate as $\sigma_x = \pm 1$. This clearly shows that, for a scalar potential $V(x)\hat{1}$ at any energy, the eigenstates are delocalized as $|\psi_{E,\sigma_x}(x)|^2 = \text{const}$.

Next, consider the case of massive chiral electrons (a kind of "1D bilayer" toy-model) described by the following Hamiltonian:

$$\hat{H}_b = k_x^2 \hat{\sigma}_x + V(x)\hat{1} \tag{A.4}$$

with $\hbar^2/(2m^*) \equiv 1$ where m^* is the effective mass (see Eq. (40) for the corresponding 2D Hamiltonian). The pseudo-spin is again a conserved quantity. However, the velocity operator is not, as it is now given by $\hat{v}_x = -i[x, \hat{H}_b] = 2k_x\hat{\sigma}_x$ and $[\hat{v}_x, \hat{H}_b] = -2i\hat{\sigma}_x dV/dx \neq 0$. When $V(x) = 0$, the eigenvectors of $\hat{H}_b$ are:

$$\psi_{k_x,\sigma_x}(x) = \frac{1}{\sqrt{2}} \begin{pmatrix} 1 \\ \sigma_x \end{pmatrix} e^{i\sigma_x k_x x}. \tag{A.5}$$

with the corresponding eigenenergies $E_{\text{kin}} = \sigma_x k_x^2$, which shows that here $\sigma_x = \text{sign}(E_{\text{kin}})$ can also be seen as the band index. When $V(x)$ is non zero, we can perform a unitary transformation to rewrite the Hamiltonian as $\tilde{H}_b = k_x^2 \hat{\sigma}_z + V(x)\hat{1}$. The eigenvalue equation then decouples in two 1D Schrödinger equations $\mp d^2\psi_\pm/dx^2 = [E - V(x)]\psi_\pm$. As for a generic potential, all states of the 1D Schrödinger equation are localized [56], it follows that the eigenstates of the "1D bilayer" Hamiltonian are also localized. This is the opposite conclusion to the "1D monolayer" case. Here the conservation of pseudo-spin leads to localization (see bottom of Fig. 12).

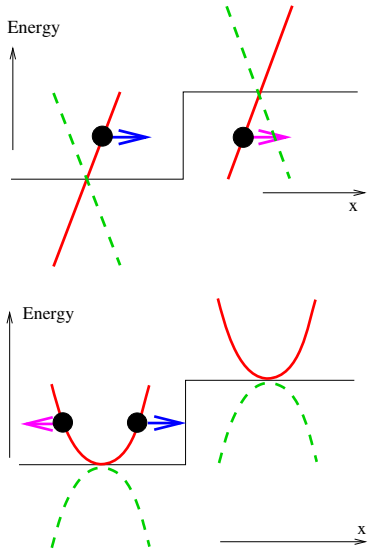

Fig. 12. Klein tunneling in one dimension. An electron incident from the left on a sharp potential step (the blue arrow indicates its direction of motion). Top: the "1D monolayer" case, in which the pseudo-spin corresponds to the direction of motion: the branch of right movers is in red $\sigma_x = +1$ and that of left movers in dashed green $\sigma_x = -1$. Bottom: the "1D bilayer" case, in which the pseudo-spin corresponds to the band index: the conduction band is in red $\sigma_x = +1$ and the valence band in dashed green $\sigma_x = -1$. In both cases, conservation of pseudo-spin imposes the direction of motion after the step (indicated by a pink arrow).

The conclusion that we draw on Klein tunneling across a step is twofold: the transition in the step is possible if (1) there are states available in the step at a matching energy (i.e. states of negative kinetic energy) and (2) if the pseudo-spin conservation permits such an inter-band transition. The latter provides a kind of selection rule, reflecting whether the appropriate matrix element for the inter-band transition vanishes or not. This matrix element (squared) is usually called the chirality factor and is given by the overlap of the incoming bispinor $(1, \sigma_x)/\sqrt{2}$ and the transmitted bispinor $(1, \sigma'_x)/\sqrt{2}$, which in 1D is

[13] Among Dirac equations, this is peculiar to the 1D case, that features no zitterbewegung.

$(1 + \sigma_x\sigma_x')/2 = \delta_{\sigma_x,\sigma_x'}$. In the case of the monolayer, the pseudo-spin is the direction of motion $\sigma_x = E_{\rm kin}/k_x$ and therefore the transition occurs with unit probability. Whereas in the bilayer case, the pseudo-spin is the band index $\sigma_x = \mathrm{sign}(E_{\rm kin})$, which would obviously change in an inter-band transition $\sigma_x' = -\sigma_x$, which is therefore strictly forbidden. These results are reminiscent of the 2D case at normal incidence where $T = 1$ for the monolayer and $T = 0$ for the bilayer [9], and the corresponding inter-band chirality factors are $(1 - \cos\pi)/2 = 1$ and $(1 - \cos(2\pi))/2 = 0$ respectively, see Section 3.1.

Note that at oblique incidence, the 2D massless case is quite unlike its 1D counterpart. In fact, for a potential with y translational invariance, there is an mapping between the massless 2D case at oblique incidence ($k_y \neq 0$) and the 1D case of Dirac electrons with a finite mass. Indeed, using the conservation of k_y, the 2D eigenvalue equation of a massless Dirac electron $(-i\hat{\sigma}_x\partial_x - i\hat{\sigma}_y\partial_y + V(x)\hat{1})\psi(x,y) = E\psi(x,y)$ becomes a 1D equation for a massive Dirac electron:

$$(-i\hat{\sigma}_x\partial_x + m\hat{\sigma}_y + V(x)\hat{1})\varphi(x) = E\varphi(x) \qquad \text{(A.6)}$$

where $\psi(x,y) = \varphi(x)\exp(ik_y y)$ defines the 1D wavefunction $\varphi(x)$ and $m \equiv k_y$ is the mass[14]. This 1D equation is actually that originally considered by Klein with $V(x) = V_0\Theta(x)$ [5] and by Sauter with $V(x) = Fx$ [57].

References

1. G. Gamow, Z. Phys. **51**, 204 (1928)
2. R.W. Gurney, E.U. Condon, Nature **122**, 439 (1928)
3. R.W. Gurney, E.U. Condon, Phys. Rev. **33**, 127 (1929)
4. A. Messiah, *Quantum mechanics* (Dover, 1999)
5. O. Klein, Z. Phys. **53**, 157 (1929)
6. A. Calogeracos, N. Dombey, Contemp. Phys. **40**, 313 (1999)
7. P.A.M. Dirac, Proc. R. Soc. Lond. **117**, 610 (1928)
8. P.A.M. Dirac, *The Principles of quantum mechanics* (Oxford University Press, 1930)
9. M.I. Katsnelson, K.S. Novoselov, A.K. Geim, Nature Phys. **2**, 620 (2006)
10. V.V. Cheianov, V. Fal'ko, Phys. Rev. B **74**, 041403 (2006)
11. J.M. Pereira, V. Mlinar, F.M. Peeters, P. Vasilopoulos, Phys. Rev. B **74**, 045424 (2006)
12. B. Huard et al., Phys. Rev. Lett. **98**, 236803 (2007)
13. R.V. Gorbachev, A.S. Mayorov, A.K. Savchenko, D.W. Horsell, F. Guinea, Nano Lett. **8**, 1995 (2008)
14. N. Stander et al., Phys. Rev. Lett. **102**, 026807 (2009)
15. A.F. Young, P. Kim, Nature Phys. **5**, 222 (2009)
16. A. Calogeracos, N. Dombey, Int. J. Mod. Phys. A **14**, 631 (1999)
17. C.W.J. Beenakker, Rev. Mod. Phys. **80**, 1337 (2008)
18. J.M. Pereira Jr, F.M. Peeters, A. Chaves, G.A. Farias, Semicond. Sci. Technol. **25**, 033002 (2010)
19. P.R. Wallace, Phys. Rev. **71**, 622 (1947)
20. C. Bena, G. Montambaux, New J. Phys. **11**, 095003 (2009)
21. A. Castro-Neto, F. Guinea, N.M.R. Peres, K.S. Novoselov, A. Geim, Rev. Mod. Phys. **81**, 109 (2009)
22. A. Geim, P. Kim, Sci. Amer. **298**, 90 (2008)
23. J.N. Fuchs, M.O. Goerbig, Pour la Science **367**, 36 (2008)
24. N.H. Shon, T. Ando, J. Phys. Soc. Jpn **67**, 2421 (1998)
25. T. Ando, T. Nakanishi, J. Phys. Soc. Jpn **67**, 1704 (1998)
26. T. Ando, T. Nakanishi, R. Saito, J. Phys. Soc. Jpn **67**, 2857 (1998)
27. E. McCann, K. Kechedzhi, V.I. Falko, H. Suzuura, T. Ando, B.L. Altshuler, Phys. Rev. Lett. **97**, 146805 (2006)
28. J.H. Bardarson, J. Tworzydlo, P. Brouwer, C.W.J. Beenakker, Phys. Rev. Lett. **99**, 106801 (2007)
29. K. Nomura, M. Koshino, S. Ryu, Phys. Rev. Lett. **99**, 146806 (2007)
30. V. Jakubský, L.M. Nieto, M.S. Plyushchay, Phys. Rev. D **83**, 047702 (2011)
31. V.V. Cheianov, V. Fal'ko, B.L. Altshuler, Science **315**, 1252 (2007)
32. J.B. Pendry, D.R. Smith, Sci. Amer. **295**, 60 (2006)
33. A.G. Aronov, G.E. Pikus, Sov. Phys. JETP **24**, 188 (1967)
34. J. Cayssol, B. Huard, D. Goldhaber-Gordon, Phys. Rev. B **79**, 075428 (2009)
35. X. Chen, J.W. Tao, Appl. Phys. Lett. **94**, 262102 (2009)
36. A.V. Shytov, M.S. Rudner, L.S. Levitov, Phys. Rev. Lett. **101**, 156804 (2008)
37. M.I. Katsnelson, Eur. Phys. J. B **51**, 157 (2006)
38. J. Tworzydlo et al., Phys. Rev. Lett. **96**, 246802 (2006)
39. E.B. Sonin, Phys. Rev. B **79**, 195438 (2009)
40. M.C. Lemme, T.J. Echtermeyer, M. Baus, H. Kurz, IEEE Electron Device Lett. **28**, 282 (2007)
41. J.R. Williams, L. DiCarlo, C.M. Marcus, Science **317**, 638 (2007)
42. B. Özyilmaz, P. Jarillo-Herrero, D. Efetov, D.A. Abanin, L.S. Levitov, P. Kim, Phys. Rev. Lett. **99**, 166804 (2007)
43. G. Liu, J. Velasco, W. Bao, C.N. Lau, Appl. Phys. Lett. **92**, 203103 (2008)
44. K.S. Novoselov, A.K. Geim, S.V. Morozov, D. Jiang, Y. Zhang, S.V. Dubonos, I.V. Grigorieva, A.A. Firsov, Science **306**, 666 (2004)
45. M.M. Fogler, D.S. Novikov, L.I. Glazman, B.I. Shklovskii, Phys. Rev. B **77**, 075420 (2008)
46. L.M. Zhang, M.M. Fogler, Phys. Rev. Lett. **100**, 116804 (2008)
47. E. Rossi, J.H. Badarson, P.W. Brouwer, S. Das Sarma, Phys. Rev. B **81**, R121408 (2010)
48. M.R. Setare, D. Jahani, Physica B Condens. Matter. **405**, 1433 (2010)
49. S. Park, H.-S. Sim, arXiv:1103.3331 (2011)
50. O. Bahat-Treidel, O. Peleg, M. Grobman, N. Shapira, M. Segev, T. Pereg-Barnea, Phys. Rev. Lett. **104**, 063901 (2010)
51. M. Ramezani Masir, P. Vasilopoulos, F.M. Peeters, Phys. Rev. B **82**, 115417 (2010)
52. C.H. Park, L. Yang, Y.W. Son, M.L. Cohen, S.G. Louie, Nature Phys. **4**, 213 (2008)
53. M. Barbier, P. Vasilopoulos, F.M. Peeters, Phys. Rev. B **80**, 205415 (2009)
54. S. Ghosh, M. Sharma, J. Phys.: Condens. Matter **21**, 292204 (2009)
55. M. Bocquet, Nucl. Phys. B **546**, 621 (1999)
56. N. Mott, W.D. Twose, Adv. Phys. **10**, 107 (1961)
57. F. Sauter, Z. Phys. **73**, 547 (1931)

[14] The familiar form of the 1D Dirac equation is recovered by the unitary transformation $(\hat{\sigma}_x, \hat{\sigma}_y, \hat{\sigma}_z) \to (\hat{\sigma}_x, \hat{\sigma}_z, -\hat{\sigma}_y)$.